Conservation and diversification of the molecular functions of YTHDF proteins

Daniel Flores-Téllez, Mathias Tankmar, Sören von Bülow, Junyu Chen, Kresten Lindorff-Larsen, Peter Brodersen* and Laura Arribas-Hernández*

University of Copenhagen, Biology Department. Ole Maaløes Vej 5, DK-2200 Copenhagen N

*Corresponding authors

Email pbrodersen@bio.ku.dk (P.B.) and laura.arribas@bio.ku.dk (L.A.-H.)

The authors declare that they have no conflict of interest

Abstract

YTHDF proteins bind to *N6*-methyladenosine (m^6A) in eukaryotic mRNA to determine many cytoplasmatic properties of target transcripts. Vertebrates encode three YTHDF proteins whose possible functional specialization is debated. In land plants, the YTHDF clade has expanded from one member in basal lineages to eleven EVOLUTIONARILY CONSERVED C-TERMINAL REGION1-11 (ECT1-11) proteins in arabidopsis, named after the conserved YTH domain placed behind a divergent intrinsically disordered region. The origin and implications of YTHDF expansion in higher plants are unknown, as only three of these eleven m^6A readers have been studied. Here, we show that stimulation of primordial cell division relies on an ancestral molecular function of the m^6A-YTHDF axis that was present in the first land plants and remained conserved over YTHDF diversification, as it appears in all major clades of YTHDF proteins in flowering plants. Nevertheless, lineage-specific neo-functionalization of ECT1, ECT9 and ECT11 happened after late duplication events, and involves altered properties mainly of the IDRs. Metazoan YTHDFs cannot provide stimulation of stem cell division in arabidopsis, suggesting different molecular activities of YTHDF proteins across kingdoms.

Introduction

N6-methyladenosine (m^6A) is the most abundant modified nucleotide occurring internally in eukaryotic mRNA. It is of major importance in gene regulation as illustrated by the embryonic lethality of mutants in the dedicated mRNA adenosine methyltransferase in higher plants (Zhong *et al*, 2008) and in mammals (Geula *et al*, 2015). The presence of m^6A in an mRNA may have multiple biochemical consequences. These include changes in the secondary structure (Liu *et al*, 2015; Roost *et al*, 2015; Spitale *et al*, 2015) and the creation of binding sites for RNA-binding proteins specialized for m^6A recognition (Dominissini *et al*, 2012; Patil *et al*, 2018). YT521-B homology (YTH) domain proteins (Stoilov *et al*, 2002) constitute the best studied class of m^6A-binding proteins (Dominissini *et al.*, 2012; Patil *et al.*, 2018; Wang *et al*, 2014a). They achieve specificity for m^6A via an aromatic pocket accommodating the *N6*-adenosine methyl group, such that the affinity of isolated YTH domains for m^6A-containing RNA is 10-20-fold higher than for unmodified RNA (Li *et al*, 2014b; Luo & Tong, 2014; Theler *et al*, 2014; Wang *et al.*, 2014a; Xu *et al*, 2014; Zhu *et al*, 2014).

Two different phylogenetic clades of YTH domains have been defined, YTHDC and YTHDF (Patil *et al.*, 2018; Zhang *et al*, 2010). Genetic studies establish that major functions of m^6A in development in both vertebrates and plants depend on the YTHDF clade of readers (Arribas-Hernández *et al*, 2018; Arribas-Hernández *et al*, 2020; Ivanova *et al*, 2017; Kontur *et al*, 2020; Lasman *et al*, 2020; Li *et al*, 2018; Shi *et al*, 2018). In all cases studied in detail thus far, plant and animal YTHDF proteins are cytoplasmic in unchallenged conditions (Arribas-Hernández *et al.*, 2018; Arribas-Hernández *et al*, 2021b; Haussmann *et al*, 2016; Lence *et al*, 2016; Scutenaire *et al*, 2018; Zhang *et al.*, 2010), and contain a long N-terminal intrinsically disordered region (IDR) in addition to the C-terminal YTH domain (Li *et al*, 2014a; Patil *et al.*, 2018; Stoilov *et al.*, 2002). While the YTH domain is necessary for specific binding to m^6A in mRNA (Li *et al.*, 2014b; Luo & Tong, 2014; Theler *et al.*, 2014; Wang *et al.*, 2014a; Xu *et al.*, 2014; Zhu *et al.*, 2014), the IDR is considered to be the effector part of the protein (Boo *et al*, 2022; Du *et al*, 2016; Park *et al*, 2019; Wang *et al.*, 2014a). Nonetheless, it has been proposed that the IDR may also participate in RNA binding, because the YTH domain alone has low affinity for mRNA (Patil *et al.*, 2018). Indeed, the IDR-dependent crosslinks between a YTHDF protein and mRNA detected upon UV-irradiation of living arabidopsis seedlings (Arribas-Hernández *et al*, 2021a) experimentally supports such a mechanism, conceptually equivalent to the contribution of IDRs in transcription factors to specific DNA binding (Brodsky *et al*, 2020).

While yeast, flies and primitive land plants encode only one YTHDF protein (Haussmann *et al.*, 2016; Lence *et al.*, 2016; Scutenaire *et al.*, 2018; Scutenaire *et al*, 2022; Varier *et al*, 2022), vertebrates have three closely related paralogs (YTHDF1-3) (Patil *et al.*, 2018; Stoilov *et al.*, 2002; Zaccara & Jaffrey, 2020; Zhang *et al.*, 2010) and higher plants encode an expanded family, with eleven members in *Arabidopsis thaliana* (*Ath*) referred to as

55 EVOLUTIONARILY CONSERVED C-TERMINAL REGION1-11 (ECT1-11) (Li *et al.*, 2014a;
56 Ok *et al*, 2005). It is a question of fundamental importance for the understanding of how
57 complex eukaryotic systems use the regulatory potential of m^6A whether these many YTHDF
58 proteins perform the same biochemical function, or whether their molecular properties are
59 specialized. Such molecular specialization could, for instance, arise as a consequence of
60 differential binding specificity to mRNA targets, distinct protein-protein interaction properties,
61 or distinct biophysical properties of IDRs, such as those related to the propensity to phase
62 separate (Bergeron-Sandoval *et al*, 2016; Borcherds *et al*, 2021). Alternatively, diversification
63 of biological functions could be achieved with distinct expression patterns or induction by
64 environmental cues, even if targets and molecular functions are the same.

65 Initial studies on mammalian cell cultures advocated a model in which YTHDF1 would
66 enhance translation of target mRNAs, YTHDF2 would promote mRNA decay, and YTHDF3
67 would be able to trigger either of the two (Li *et al*, 2017; Shi *et al*, 2017; Wang *et al.*, 2014a;
68 Wang *et al*, 2015). Nonetheless, recent studies in mouse, zebrafish and human cell culture
69 involving single and combined *ythdf* knockouts and analysis of interacting mRNAs and
70 proteins do not support functional specialization, and propose a unified molecular function for
71 all three vertebrate YTHDFs in accelerating mRNA decay (Kontur *et al.*, 2020; Lasman *et al.*,
72 2020; Zaccara & Jaffrey, 2020).

73 The great expansion of YTHDF proteins in higher plants is unique among eukaryotes
74 (Stoilov *et al.*, 2002). Phylogenetic analyses of plant YTHDF domains have established the
75 existence of 3 clades in angiosperms, DF-A (comprising *Ath* ECT1, ECT2, ECT3, ECT4), DF-
76 B (comprising *Ath* ECT5, ECT10, ECT9), and DF-C (comprising *Ath* ECT6, ECT7, ECT8 and
77 ECT11) (Scutenaire *et al.*, 2018). The fact that the eleven arabidopsis paralogs have the
78 aromatic residues necessary for specific binding to m^6A (Fray & Simpson, 2015) suggests
79 that they may all function as m^6A readers. The unified model for YTHDF function recently
80 proposed for the three vertebrate paralogs (Kontur *et al.*, 2020; Lasman *et al.*, 2020; Zaccara
81 & Jaffrey, 2020) is consistent with what had already been established for *Ath* ECT2, ECT3
82 and ECT4 in the plant DF-A clade (Arribas-Hernández *et al.*, 2018), even though the three
83 plant paralogs are more divergent in sequence than the highly similar mammalian YTHDF1-3
84 (Arribas-Hernández *et al.*, 2018; Stoilov *et al.*, 2002; Zaccara & Jaffrey, 2020). The two most
85 highly expressed members in *A. thaliana*, ECT2 and ECT3, accumulate in dividing cells of
86 organ primordia and exhibit genetic redundancy in the stimulation of stem cell proliferation
87 during organogenesis (Arribas-Hernández *et al.*, 2018; Arribas-Hernández *et al.*, 2020). The
88 two proteins probably act truly redundantly *in vivo* to control this process, because they
89 associate with highly overlapping target sets in wild type plants, and each exhibits increased
90 target mRNA occupancy in the absence of the other protein (Arribas-Hernández *et al.*, 2021b).
91 Simultaneous knockout of *ECT2* and *ECT3* causes a 2-day delay in the emergence of the first

true leaves, aberrant leaf morphology, slow root growth and defective root growth directionality among other defects (Arribas-Hernández *et al.*, 2018; Arribas-Hernández *et al.*, 2020) that resemble those of plants with diminished m^6A deposition (Bodi *et al*, 2012; Růžička *et al*, 2017; Shen *et al*, 2016). For the third DF-A clade member, *ECT4*, the genetic redundancy is only noticeable in some tissues as an exacerbation of *ect2/ect3* phenotypes upon additional mutation of *ect4*, most conspicuously seen in leaf morphogenesis (Arribas-Hernández *et al.*, 2018; Arribas-Hernández *et al.*, 2020). Despite the strong evidence for redundant functions among these three YTHDF paralogs in the DF-A clade, the presence of many other YTHDF proteins in arabidopsis leaves open the question of whether substantial functional specialization of YTHDF proteins exists in plants.

In this study, we systematically define overlaps in molecular functions of plant YTHDF proteins. Employing functional complementation of leaf formation in triple *ect2/ect3/ect4* (*te234*) mutants, we demonstrate that at least one member of all clades in arabidopsis, and the only YTHDF protein from a group of primitive land plants, are able to replace ECT2/3/4 functions. In contrast, a few late-diverging ECTs were not able to perform the molecular functions of ECT2/3/4. Based on these results, we propose an ancestral molecular role for land plant YTHDF proteins in stimulation of primordial cell proliferation, and sustained functional redundancy during the diversification process that started more than 400 million years ago (Mya). In addition, our results also support the functional divergence of a small subset of fast-evolving plant YTHDF proteins with contributions to specialization mainly from the IDRs, but also from the YTH domains.

Results

The phylogeny of plant YTHDF proteins comprises several clades

The adaptation of plants to terrestrial life, since the transition from freshwater to land until the rise of angiosperms, was accompanied by the acquisition of morphological, physiological and genomic complexity (One Thousand Plant Transcriptomes, 2019; Pires & Dolan, 2012). Knowing how diversification of YTHDF proteins came about during the course of plant evolution is relevant to understand their distinct functions, and may hint at roles they might have played in this process. However, the species included in the so far most detailed phylogenetic study on plant YTHDF proteins jump from bryophytes (mosses, liverworts and hornworts (Harris *et al*, 2020; Li *et al*, 2020; One Thousand Plant Transcriptomes, 2019; Puttick *et al*, 2018; Su *et al*, 2021; Zhang *et al*, 2020b)) to angiosperms (flowering plants) (Scutenaire *et al.*, 2018). To include the YTHDF repertoires of intermediately diverging clades such as ferns and

127 gymnosperms, we performed a phylogenetic analysis using YTHDF proteins from taxa
128 widely spread across terrestrial plant evolution (Fig. 1A). When possible, we included
129 basal clades of each group in addition to model organisms. The resulting phylogenetic
130 tree largely agrees with the DF-A/B/C clades defined on the basis of angiosperm
131 YTHDF sequences (Scutenaire *et al.*, 2018), with some minor differences. We
132 consider that the former DF-C group comprising *Ath* ECT6/7/8/11 (Scutenaire *et al.*,
133 2018) can be subdivided into two groups that diverged early during YTHDF radiation
134 (approximate likelihood-ratio test (aLRT) = 87), because the split between them is
135 comparable to that of clades DF-A and -B (Fig. 1B). Thus, we introduced the name
136 'DF-D' for the clade defined by one *Amborella trichopoda* (a basal angiosperm)
137 YTHDF protein (*Atr* DFD) and *Ath* ECT6/7 (Fig. 1B). Furthermore, since the group
138 comprising bryophyte YTHDFs did not receive a designation in previous studies, we
139 named it DF-E (mnemotechnic for 'Early') (Fig. 1B). Finally, an additional group
140 composed of early-diverging YTHDF proteins from the fern *Ceratopteris richardii* (*Cri*
141 DF1/2/3) and the gymnosperm *Ginkgo biloba* (*Gb* DF1/2) was named DF-F, as it did
142 not fall into any of the other clades (Fig. 1B). We conclude that land plant YTHDFs are
143 phylogenetically more diverse than previously appreciated.
144
145 *YTHDF protein diversification occurred early during land plant evolution*
146 Our phylogenetic analysis shows that plant YTHDF diversification started at least
147 before the radiation of Euphyllophytes (plants with true leaves comprising ferns,
148 gymnosperms and angiosperms) more than 410 Mya (Magallón *et al*, 2013; Su *et al.*,
149 2021). This is because bryophytes possess one or two YTHDFs in the 'early clade'
150 (DF-E) while the fern *C. richardii* has six YTHDFs in 3 different clades (Fig. 1B). Thus,
151 our analysis reveals that YTHDF radiation started early in land plant evolution and coincided
152 with the acquisition of morphological complexity and the adaptation to diverse environments.
153
154 *A functional complementation assay for plant YTHDF proteins*
155 To address the degree of functional specialization among plant YTHDF proteins in a simple
156 manner, we set up a functional complementation assay that scores the ability of each of the
157 eleven arabidopsis YTHDF proteins (Fig. 2A) to perform the molecular functions of ECT2/3/4
158 required for rapid cellular proliferation in leaf primordia. Initial attempts at using the *ECT2*
159 promoter for ectopic *ECT* expression in primordial cells were unsuccessful, as pilot
160 experiments with a genomic *ECT4* fragment revealed that its expression was substantially

161 lower than that of a similar *ECT2* genomic fragment when driven by the *ECT2* promoter (Fig.
162 S1), perhaps pointing to the presence of internal *cis*-regulatory elements. We therefore turned
163 to the use of *ECT* cDNAs (c*ECT*s) under the control of the promoter of the ribosomal protein-
164 encoding gene *AthuS7B*/*RPS5A* (At3g11940 (Lan *et al*, 2022)) active in dividing cells (Weijers
165 *et al*, 2001) in a pattern that resembles the *ECT2/3/4* expression domain (Arribas-Hernández
166 *et al.*, 2018; Arribas-Hernández *et al.*, 2020). Transformation of the *uS7Bp:cECT2-mCherry*
167 construct in *te234* plants resulted in complementation frequencies of ~40-50% among primary
168 transformants, a percentage slightly lower but comparable to that obtained with the genomic
169 *ECT2-mCherry* construct under the control of *ECT2* promoter and terminator regions
170 (*ECT2p:gECT2-mCherry*) (Arribas-Hernández *et al.*, 2018) (Fig. S2A). Free mCherry
171 expressed from a *uS7Bp:mCherry* transgene showed no complementation (Fig. S2A), as
172 expected. Importantly, the leaf morphology and the pattern of mCherry fluorescence in
173 *uS7Bp:cECT2-mCherry* lines was indistinguishable from that of *ECT2p:gECT2-mCherry* (Fig.
174 S2B). Hence, we proceeded with expression of cDNAs encoding all of ECT1-11 fused to C-
175 terminal mCherry under the control of the *uS7B* promoter (henceforth ECT1-11) in *te234*
176 mutants (Fig. 2B).
177
178 *Percentage of complementation among primary transformants as a readout for functionality*
179 To design the experimental approach in detail, we considered the fact that expression of
180 transgenes involves severe variations in levels and patterns among transformants. This is due
181 to positional effects of the T-DNA insertion and the propensity of transgenes to trigger silencing
182 in plants (Fagard & Vaucheret, 2000), and explains why only a fraction of *ECT2-mCherry* lines
183 rescues loss of ECT2 function (Fig. S2A, (Arribas-Hernández *et al.*, 2018)). Hence, many
184 independent lines need to be analyzed before choosing stable and representative lines for
185 further studies. Taking this into account, we decided to perform systematic and unbiased
186 comparisons of ECT functionality by counting the fraction of primary transformants (henceforth
187 T1s) able to complement the late leaf emergence of *te234* plants for each construct. We set
188 a size threshold for the rapid assessment of large numbers of transformants considering that
189 leaves longer than 0.5 mm after 10 days of growth constitute unambiguous sign of
190 complementation, because this is the minimum size never reached by *te234* or control lines
191 (Fig. S2B). Hence, we calculated complementation percentages as the number of T1s with
192 leaf size (s) larger than 0.5 mm relative to the total number of transformants, and averaged
193 that score over several independent transformations (Figs. 2C, S3A, and S4A).
194
195 *Most arabidopsis YTHDF paralogs can perform the molecular function required for leaf*
196 *development*

197 The results of the comparative analysis reveal a high degree of functional overlap within the
198 arabidopsis YTHDF family, because eight out of the eleven YTHDF proteins, namely
199 ECT2/3/4/5/6/7/8/10, are able to complement delayed leaf emergence of *ect2/3/4* mutants
200 with frequencies ranging from 14% (ECT6) to 39% (ECT2) when expressed in the same cells
201 (Figs. 2C and S4A). Importantly, complementation is indirect proof of m^6A-binding ability,
202 because the proteins must bind to the targets whose m^6A-dependent regulation is necessary
203 for correct leaf organogenesis in order to restore ECT2/3/4 function (Arribas-Hernández *et al.*,
204 2018). This conclusion is not trivial, as some eukaryotes lacking canonical m^6A-
205 methyltransferases encode YTH domain proteins (Balacco & Soller, 2019) and, indeed, the
206 YTH domain of fission yeast Mmi1 does not bind to m^6A (Wang *et al*, 2016). Thus, most, but
207 not all, arabidopsis YTHDF proteins retain the molecular functions required to stimulate
208 proliferation of primed stem cells. Of the three remaining proteins, ECT1 showed only residual
209 complementation capacity, while no complementation was observed for ECT11 at this stage
210 (Figs. 2C and S4A). Finally, we could not conclude at this point whether ECT9 could replace
211 ECT2/3/4 function or not, because this transgene produced very few transformants in the
212 *te234* background (Figs. 2C, S3A and S5) with barely visible fluorescence. All such
213 transformants underwent complete silencing in the following generation (T2).
214
215 *Differences in complementation scores are not explained by a bias in expression levels*
216 Our T1 scoring method relies on the assumption that the *uS7B* promoter drives similar ranges
217 of expression of the different *ECT* cDNAs. However, different silencing propensities between
218 the *ECT* cDNAs might introduce bias in the results. To take this possibility into account, we
219 first performed western blotting from three lines per transgene selected as the best-
220 complementing in their group (Fig. S4B). The results showed that the higher complementation
221 scores of e.g. ECT2, ECT3 and ECT8 are not explained by higher expression. Rather, the
222 reverse was true. For example, while ECT2 could complement *te234* plants with the lowest
223 expression among all ECTs, the few lines expressing ECT1 able to pass the complementation
224 threshold had the highest expression of all ECTs, suggesting that ECT1 can only partially
225 compensate for loss of ECT2/3/4 when overexpressed.
226
227 *The same functional classes of ECTs emerge from complementation of silencing-deficient*
228 *te234*
229 Next, we tested whether the same results could be reproduced in plants lacking *RNA-*
230 *DEPENDENT RNA POLYMERASE 6* (*RDR6*), a gene essential for the biogenesis of
231 transgene-derived short interfering RNAs (siRNAs) (Dalmay *et al*, 2000; Mourrain *et al*, 2000).
232 Because siRNA-guided transgene silencing is impaired in *rdr6* mutants, higher and more
233 homogenous ranges of expression among different transgenes can be expected in this

234 background. Hence, we constructed *rdr6-12/te234* mutants that exhibited both the narrow,
235 downward-curling leaf phenotype of *rdr6* mutants (Peragine *et al*, 2004) and the characteristic
236 rosette morphology of *te234* (Arribas-Hernández *et al.*, 2018) (Fig. S6A). Importantly, the
237 delay in leaf emergence was identical in *te234* and *rdr6-12/te234* mutants (Fig. S6A) and the
238 complementation rates of *ECT2* transgenes were much higher in the silencing-deficient plants
239 (Fig. S2A), indicating that the <100% complementation frequencies in *te234* were indeed due
240 to RDR6-dependent silencing. In the *rdr6*/*te234* background, complementation scores of the
241 eight functionally equivalent ECTs (ECT2/3/4/5/6/7/8/10) ranged from 59% (ECT6) to 94%
242 (ECT2), and the differences between these ECTs were less pronounced, but followed a trend
243 largely unchanged compared to the *te234* background (Fig. 2C,D). On the other hand, the
244 difference between the eight ECTs with ECT2/3/4-like function and the group of ECTs with
245 negligible complementation capacity (ECT1/9/11) was highlighted by the *rdr6* mutation: ECT1
246 and ECT11 did not increase their scores (Fig. 2D), and absence of silencing resulted in a
247 number of *ECT9* transformants with visible mCherry fluorescence, yet no complementation
248 activity (Figs. 2D and S6B), thus verifying the lack of ECT2/3/4-like function of ECT9.
249
250 *Rosette phenotypes corroborate the complementation scores*
251 To verify the results of the complementation assay in the adult phenotype, we characterized
252 rosettes of two independent lines for each transgene (Fig. 2E-H). As expected, *rdr6-12/te234*
253 plants expressing ECTs with high complementation scores resembled single *rdr6-12* mutants
254 (Fig. 2E,F), while the ECT1 and ECT11 transformants with the biggest first true leaves at 10
255 DAG produced plants only slightly bigger than the *rdr6-12/te234* background (Fig. 2E,G),
256 indicating low but residual ECT2/3/4-like function for these two proteins. Strikingly, *rdr6-*
257 *12/te234* plants expressing ECT9 exhibited strong developmental phenotypes (Figs. 2H and
258 S6B) that resembled those of severely m^6A-depleted plants (Růžička *et al.*, 2017; Shen *et al.*,
259 2016). Such an effect was not observed for any other *Ath* ECT. This result suggests that ECT9
260 can bind to m^6A targets, either exerting opposite molecular actions compared to ECT2/3/4, or
261 simply precluding their possible regulation by remaining ECTs such as ECT5/6/7/8/10 by
262 competitive binding. We tested whether ECT9 can outcompete endogenous ECT2/3/4 in the
263 proliferating cells of the apex by expressing the ECT9 transgene in single *rdr6-12* mutant
264 plants. We found no evidence for this, because the transformation produced a high amount of
265 fluorescent T1s without obvious defects (Fig. S7).
266 Altogether, our results indicate that arabidopsis YTHDF proteins may be divided into three
267 functional classes, i) ECT2/3/4/5/6/7/8/10 with the molecular functionality of ECT2/3/4 required
268 for correct and timely leaf formation; ii) ECT1/11, with only residual ECT2/3/4 functions, and
269 iii) ECT9, unable to perform such functions and toxic when present in the expression domain
270 of ECT2/3/4 in their absence.

271

272 *Validation of the functional assay by loss-of-function genetic analysis*

273 One of the predictions of the genetic interactions between *ECT* genes that can be drawn from
274 our results is particularly unexpected and, therefore, suitable for the validation of our
275 complementation assay by classical genetic analysis: Mutation of *ECT1* should not exacerbate
276 the developmental defects of *te234*, even if it is endogenously expressed in leaf primordia.
277 *ECT1* is especially suitable for validation for two reasons. First, ECT1 is the closest paralog
278 of ECT2/3/4 in arabidopsis (Fig. 1B), intuitively suggesting some degree of genetic
279 redundancy. Second, *ECT1* promoter-reporter fusions (Ok *et al.*, 2005) and mRNA-seq data
280 (Fig. S9, Zhang *et al*, 2020a) suggest that expression levels and tissue specificity of *ECT1* are
281 comparable to that of *ECT4*, whose activity is easily revealed as an enhancer mutant of
282 *ect2/ect3* (Arribas-Hernández *et al.*, 2018).

283

284 *ECT1 and ECT2/3/4 are cytoplasmic and are expressed in the same cell types*

285 We first assessed the expression pattern and subcellular localization of ECT1 using stable
286 transgenic lines expressing TFP translationally fused to the C-terminus of *ECT1* (*ECT1-TFP*,
287 Fig. S10A). The pattern of turquoise fluorescence was strongly reminiscent of that of
288 fluorescent ECT2/3/4 fusions (Arribas-Hernández *et al.*, 2018) with signal at the base of young
289 leaves, in leaf primordia, main root tips and lateral root primordia at different stages (Fig. 3A-
290 D). In addition, confocal microscopy of meristematic root cells showed cytoplasmic ECT1-TFP
291 signal with heterogenous texture similar to ECT2/3/4 (Arribas-Hernández *et al.*, 2018) (Fig.
292 3E). We noticed, however, that most root tips had a few cells containing distinct ECT1-TFP
293 foci (Fig. 3F) in the absence of stress. We found no trace of free TFP that could be causing
294 imaging artifacts (Fig. S10A), but note that the *ECT1-TFP* transgenic lines selected on the
295 basis of visible and reproducible pattern of fluorescence may overexpress *ECT1* (Fig. S10B).
296 We conclude from the similar expression pattern and subcellular localization of ECT1 and
297 ECT2/3/4 that assessment of the possible exacerbation of *te234* phenotypes by additional
298 loss of *ECT1* function is a meaningful test of our functional assay.

299

300 *Mutation of ECT1 does not exacerbate the phenotype of ect2/ect3/ect4 plants*

301 We isolated three homozygous knockout lines caused by T-DNA insertions in the *ECT1* gene,
302 *ect1-1*, *ect1-2*, and *ect1-3* (Fig. 3G,H), and crossed two of them to different *ect2/ect3/ect4*
303 triple mutants to obtain two independent allele combinations of quadruple *ect* mutants, *ge1234*
304 and *Gge1234* (Fig. S10C). In both cases, the quadruple mutant plants were indistinguishable
305 from the corresponding *te234* and *Gte234* triple mutant parentals (Figs. 3I and S10C,D).
306 Similarly, triple *ect1/ect2/ect3* mutants were identical to double *ect2/ect3* mutants, and single
307 *ect1* mutants did not show any obvious defects in *ect2/3*-associated traits such as leaf or root

308 organogenesis and trichome branching (Figs. 3I and S10D-F). Thus, despite their similar
309 expression pattern, there is no indication of redundancy between ECT1 and the other three
310 DF-A clade paralogs. This unexpected conclusion agrees with the poor ECT2/3/4-like activity
311 of ECT1 in our functional assay, thereby validating the approach.
312
313 *The divergent function of ECT1 and ECT11 is caused mainly by properties of their IDRs*
314 Having established that different molecular functions are represented in the arabidopsis
315 YTHDF family, we went on to map the molecular regions responsible for this functional
316 divergence. First, we investigated whether lack of *te234* mutant complementation by
317 ECT1/9/11 is due to altered target binding by the YTH domain, IDR-related effector functions,
318 or a combination of both. Thus, we built chimeric IDR/YTH constructs between ECT2 and
319 ECT1/9/11 (Fig. 4A). We also tested an ECT8$_{IDR}$/ECT2$_{YTH}$ chimera (C-8/2) to assess whether
320 hybrid constructs can at all be functional, choosing ECT8 as a positive control due to its robust
321 complementation of seedling and adult phenotypes (Fig. 2C,D,F). Expression of the constructs
322 in *te234* mutants showed that the C-8/2 chimera was fully functional (Figs. 4B, S3B and S8),
323 thus validating the approach. In contrast, ECT1- and ECT11-derived chimeras proved that
324 both the IDR and the YTH domain of these two proteins only retain a reduced degree of
325 function compared to the equivalent regions in ECT2 (Figs. 4B, S3B and S8). In particular, the
326 IDRs of both proteins scored lower than their YTH domains when combined with the other half
327 from ECT2 (Fig. 4B), pointing to divergence in the IDR as the main cause for different
328 functionality. In wild type ECT1 and ECT11 proteins, the combination of the two poorly-
329 performing parts is likely the cause for the minute ECT2/3/4-like activity.
330
331 *The IDR of ECT9 is incapable of performing ECT2/3/4 molecular functions, but its YTH domain*
332 *retains some ECT2/3/4-like function*
333 The ECT2$_{IDR}$/ECT9$_{YTH}$ chimera (C-2/9) yielded normal transformation efficiencies and up to
334 17% of T1s had signs of complementation compared to 56% for ECT2 (Figs. 4B, S3B and
335 S8), suggesting that the YTH domain of ECT9 retains at least partial functionality. However,
336 the reverse construct (ECT9$_{IDR}$/ECT2$_{YTH}$, C-9/2) recapitulated the results obtained for ECT9:
337 low transformation efficiency and low fluorescence in the few T1s recovered, and complete
338 silencing in the next generation (Figs. 4B, S3B and S8). Hence, we introduced the C-9/2
339 chimera into the *rdr6-12/te234* background and observed plants with stronger fluorescence
340 exhibiting aberrant morphology, again similar to what was obtained with ECT9 (Figs. 4C,D,
341 S3C and S6B). These results confirm that ECT9 is not functionally equivalent to ECT2/3/4,
342 and point to the IDR as the main site of functional divergence of the protein.
343
344 *The molecular requirements for m^{6}A-binding are conserved in the YTH domains of ECT1/9/11*

345 To pinpoint molecular characteristics of ECT1/9/11 responsible for their different functionality,
346 we performed a series of comparative analyses between ECT1/9/11 and other ECT proteins.
347 We first analyzed the YTH domains, taking ECT2 as a reference and using the structurally
348 well-characterized YTH domain of *Homo sapiens* (*Hs*) YTHDF1 in complex with RNA
349 GGm^{6}ACU (Xu *et al*, 2015) as a model. Amino acid sequence alignment of the YTH domains
350 of all arabidopsis ECTs (Fig. S11), AlphaFold-predictions (Jumper *et al*, 2021; Varadi *et al*,
351 2022) of the apo structures (Fig. S12) and homology models (Biasini *et al*, 2014) of the m^{6}A-
352 bound state confirmed a high degree of conservation of the key residues required for m^{6}A-
353 RNA binding and overall fold of the YTH domain of ECT1/9/11, in agreement with the partial
354 functionality observed in our chimeric constructs (Fig. 4B). However, we also detected a few
355 non-conservative amino acid substitutions specific for ECT1/9/11 (Figs. 5A and S11),
356 preferentially located on the surface of the protein but far from the RNA-binding groove (Fig.
357 S12). These non-conservative substitutions are prime candidates to explain the minor
358 differences in functionality, a scenario that implies biological functions of YTH domains other
359 than mere m^{6}A-binding capacity.
360
361 *The IDRs of ECT1/9/11 have biophysical properties distinct from ECT2/3/4/5/6/7/8/10*
362 We next focused on the N-terminal regions of *ECT1/9/11.* Because protein disorder
363 predictions using MobiDB (Piovesan *et al*, 2023) confirmed that they are all disordered (Fig.
364 S13), we used approaches suitable for the study of IDRs. Prediction of short linear motifs
365 (SLiMs) that may mediate interaction with effector proteins gave many possibilities that did not
366 follow any clear pattern when compared between the different ECT classes (Fig. S13). Hence,
367 we decided to study other properties known to be important in IDRs and focused on the
368 propensity to form liquid condensates, the amino acid composition, and the distribution of
369 charge. ECT2 can form condensates *in vitro* (Arribas-Hernández *et al.*, 2018), and localizes
370 *in vivo* to distinct foci upon stress (Arribas-Hernández *et al.*, 2018; Scutenaire *et al.*, 2018),
371 identified as stress granules (Scutenaire *et al.*, 2018). Similar properties have been reported
372 for human YTHDFs, which engage in liquid-liquid phase transition when concentrated on
373 polyvalent m^{6}A-modified target RNA *in vitro* (Fu & Zhuang, 2020; Gao *et al*, 2019; Ries *et al*,
374 2019; Wang *et al*, 2020). To determine whether the distinct functional classes of ECTs differed
375 in their propensity to phase separate, we employed a recently developed coarse-grained
376 model of IDRs with residue-specific parameters estimated from experimental observations of
377 many IDRs (Tesei *et al*, 2021) to simulate their tendency to remain in the condensed phase
378 or disperse in solution. As control, we used the well-studied IDR of the human RNA-binding
379 protein Fused in Sarcoma (FUS) (Kato *et al*, 2012; Kato & McKnight, 2021; Patel *et al*, 2015;
380 Schwartz *et al*, 2013). The results showed that the IDR of ECT2 has a clear propensity to
381 remain in the condensed phase (Fig. 5B-C and Movie S1) with a highly favorable Gibb's free

382 energy change for the transition from dilute aqueous solution to condensed phase (Fig. 5D),
383 comparable to, albeit not as pronounced as for the IDR of FUS (Fig. 5B-D). While the IDRs of
384 most ECT proteins behaved comparably to ECT2, the IDRs of ECT1 and ECT11 were clear
385 outliers (Figs. 5B-D and S14A). Compared to all other ECTs, the IDR of ECT1 showed a much
386 stronger propensity to phase separate, consistent with the spontaneous granule formation of
387 ECT1-TFP *in vivo* (Figs. 3F and 4B-D, and Movie S2). On the contrary, the IDR of ECT11
388 dispersed into solution much more readily (Fig. 5B-D and Movies S3). Thus, the IDRs of ECT1
389 and ECT11 have markedly different biophysical properties from those of ECT2/3/4/5/6/7/8/10,
390 perhaps contributing to their different functionality *in vivo*. In contrast, the IDR of ECT9 did not
391 stand out from the rest in the simulations of phase separation propensity. We also note that
392 the different phase separation propensity among the ECTs is driven, in the main, by their
393 different content of sticky residues as defined by the CALVADOS model (Tesei *et al.*, 2021)
394 (Fig. S14B). In this context, it is potentially of interest that ECT1, ECT9 and ECT11 all have a
395 higher content of Phe residues than the nearly Phe-depleted IDRs of ECT2/3/4/5/6/7/8/10 (Fig.
396 S14C). For ECT1, whose Tyr and Trp enrichment is comparable to that of ECT2/3/4/5/6/7/8/10
397 (Fig. S14C), the additional enrichment of the similarly sticky Phe may contribute to its more
398 pronounced phase separation propensity, but it is unclear what, if any, the functional
399 consequence of Phe enrichment in the Tyr/Trp-poor IDRs of ECT9 and ECT11 may be.
400 We finally analyzed the charge distribution, as this may dictate properties such as
401 compactness and shape of IDR conformations (Bianchi *et al*, 2022; Das *et al*, 2016). We found
402 that the IDRs of ECT2/3/4/5/6/7/8/10 show a recurrent pattern with accumulation of net
403 negative charge towards the N-terminus, and recovery to near-neutrality closer to the YTH
404 domain (Figs. 5E and S14D). The IDRs of ECT1, ECT9 and ECT11 differ from this pattern,
405 but in distinct ways: ECT1 does not show a pronounced patterning of the charged residues,
406 while ECT9 increasingly accumulates negative charge (Figs. 5E) and ECT11 increasingly
407 accumulates positive charge (Fig. S14D). It is an interesting possibility, therefore, that charge
408 separation in the IDR is a requirement to fulfill the molecular functions of ECTs to accelerate
409 growth in primordial cells.
410
411 *The ability to complement ect2/3/4 does not simply follow affiliation with phylogenetic clades*
412 We next compared the functional groups of YTHDF proteins defined by our complementation
413 assays with the YTHDF phylogeny. Strikingly, the ability to rescue defective timing of leaf
414 emergence does not follow the defined phylogenetic clades, because both high and low/null
415 complementation capacities are present in the same clades. For example, ECT2, ECT5 and
416 ECT8 in clades DF-A, -B and -C respectively present high ECT2/3/4-like functionality, while
417 ECT1, ECT9 and ECT11 in these same clades do not (Figs. 1B and 2C-H). It is noteworthy,
418 however, that there is a clear trend for non-complementors to be the most highly divergent

419 proteins in each group, as revealed by the length of the branches in the phylogenetic tree (Fig.
420 1B). Indeed, the longest branches in both our tree (highlighted in red in Fig. 1B) and the one
421 in the study by Scutenaire et al. (2018) correspond to ECT1, ECT9, and ECT11, which also
422 have the highest number of amino acid substitutions compared to the only YTHDF protein of
423 the liverwort *Marchantia polymorpha* (*Mpo* YTHDF) (Bowman *et al*, 2017) (Fig. 6A). These
424 results suggest that the common ancestor of YTHDF proteins in land plants may have had a
425 molecular function related to that of the modern arabidopsis ECT2/3/4, and that this function
426 has been conserved in the least-divergent members of the DF-A/B/C/D clades. Subsequent
427 duplication and neofunctionalization may have driven the rapid evolution of highly-divergent
428 YTHDF proteins (ECT11, ECT1, and ECT9 in Arabidopsis) that have lost their primary function
429 and perhaps fulfill different molecular roles in the plant m^6A pathway.
430
431 *The molecular function of ECT2/3/4 was present in the first land plants*
432 To test whether the common ancestor of plant YTHDF proteins indeed had a molecular
433 function similar to that of the modern *Arabidopsis* ECT2/3/4, we subjected *Mpo* YTHDF (Fig.
434 2A) to our functional assay, as bryophytes are the earliest-diverging taxon of land plants (Fig.
435 1A, (Harris *et al.*, 2020; Li *et al.*, 2020; One Thousand Plant Transcriptomes, 2019; Puttick *et*
436 *al.*, 2018; Su *et al.*, 2021; Zhang *et al.*, 2020b)). The result showed a partial, but clear capacity
437 of two different splice forms of *Mpo* YTHDF to complement the delay in leaf emergence and
438 morphology defects of arabidopsis *te234* plants (Figs. 6B, S3D and S15A,B). Although the
439 complementation scores were low (Fig. 6B), a thorough inspection of the fluorescence
440 intensity in all primary transformants revealed that the transgene was only expressed very
441 weakly in a reduced subpopulation of plants, possibly be due to the tendency to trigger
442 silencing upon heterologous expression of a long cDNA from a distant plant species (Wang &
443 Roossinck, 2006). We therefore introduced the best-complementing isoform into *rdr6-*
444 *12/te234* mutants. This approach yielded a much higher complementation score of 52% (Fig.
445 6C), and plants very similar to those expressing ECT2 in the same background (Figs. 6D and
446 S6B). Gratifyingly, the simulations of the behavior of the IDR of *Mpo* YTHDF showed phase
447 separation propensity and charge pattern similar to the ECT2/3/4/5/6/7/8/10 group, further
448 substantiating that these IDR characteristics correlate with the ability to fulfill ECT2/3/4
449 function in leaf formation (Fig. 6E-H), Hence, our results demonstrate that the core molecular
450 activity of *Ath* ECT2/3/4 was present in the first land plants, and suggest that stimulating
451 proliferation of primed stem cells is the ancestral YTHDF molecular function in plants.
452
453 *Heterologous expression of animal YTHDFs enhances the phenotype caused by loss of*
454 *ECT2/3/4 in Arabidopsis*

455 Finally, we subjected *Hs* YTHDF2 and *Drosophila melanogaster* (*Dm*) YTHDF (Fig. 2A) to our
456 functional assay to test whether they could function molecularly like plant YTHDFs. While we
457 did not observe complementation of the delayed leaf emergence of *te234* plants in any of the
458 transformants (Fig. 6B), several *Hs* YTHDF2 lines showed more acute developmental defects
459 compared to *te234* (Fig. S15B). Although these defects were not observed among *Dm* YTHDF
460 lines, no expression could be detected in these plants either. Hence, we repeated the
461 transformation in the *rdr6-12/te234* background, this time obtaining numerous transformants
462 of both *Dm* YTHDF and *Hs* YTHDF2 with strong fluorescence (Figs. 6C and S6B). These
463 plants showed aberrant morphology comparable to the effect caused by expression of ECT9
464 and C-9/2, with resemblance to arabidopsis mutants with severe depletion of m^6A (Růžička *et*
465 *al.*, 2017; Shen *et al.*, 2016) (Figs. 6D and S6B). Thus, expression of metazoan YTHDFs in
466 arabidopsis *ECT2/3/4*-deficient plants exacerbates their developmental phenotype. This result
467 is in agreement with the generally accepted idea that m^6A/YTHDF2 destabilize mRNA in
468 mammals (Herzog *et al*, 2017; Ke *et al*, 2017; Sommer *et al*, 1978; Wang *et al.*, 2014a; Wang
469 *et al*, 2014b) while m^6A/ECT2/3/4 do the opposite in plants (Anderson *et al*, 2018; Arribas-
470 Hernández *et al.*, 2021b; Parker *et al*, 2020; Shen *et al.*, 2016; Wei *et al*, 2018). However, an
471 analogous molecular mechanism between plant and animal YTHDFs cannot be completely
472 ruled out, because a different cellular context may be hampering the molecular activity of
473 metazoan YTHDFs in plant cells, and simple competition for targets with remaining ECTs
474 could be the cause of the enhanced phenotype. Nonetheless, we note that the IDRs of *Hs*
475 YTHDF2 and *Dm* YTHDF had much weaker phase separation propensity and different charge
476 distribution compared to ECT2 (Fig. 6E-G), perhaps contributing to the lack of ECT2/3-like
477 function *in planta*.
478
479 **Discussion**
480 *Functional versus biological redundancy*
481 Our study reveals that most YTHDF proteins in higher plants can perform, essentially, the
482 same molecular functions that allow ECT2/3/4 to promote stem cell proliferation and control
483 organogenesis. We anticipate that this molecular function may be used in specific biological
484 contexts by ECT5/6/7/8/10 due to different expression patterns and response to stimuli,
485 thereby achieving biological specialization with respect to ECT2/3/4. Such variability can
486 already be inferred from available RNA-Seq data in the arabidopsis eFP Browser
487 (BAR.toronto.ca) that show, for example, that ECT8 is primarily expressed during
488 senescence-associated processes, perhaps in connection to re-growth after reversible
489 proliferative arrest (Gan, 2003; Wuest *et al*, 2016). In addition to redundancy, there is a clear
490 pattern of lineage-specific specialization in fast-evolving YTHDF proteins from different clades,
491 exemplified in arabidopsis by ECT1, ECT11, and most prominently ECT9. Whether these

492 proteins act to counteract the ECT2/3/4-like function by competing for m^6A-containing
493 transcripts, perhaps halting growth upon stress, or whether they perform independent
494 functions in different tissues or cell types, is open for new investigations.
495
496 *ECT1 is a newly evolved gene in a Brassicaceae lineage*
497 Surprisingly, the only member of the DF-A clade not yet characterized as m^6A reader, ECT1,
498 scored low in our functional assay and indeed, inactivation of *ECT1* does not enhance the
499 phenotype caused by loss of *ECT2/3/4* despite expression of *ECT1* in the same cell types and
500 subcellular compartment as the other DF-A paralogs. We note that a previous description of
501 nuclear and cytoplasmic fluorescence of a *35Sp:ECT1-GFP* fusion (Ok *et al.*, 2005) may be
502 due to the fact that the authors used epifluorescence instead of confocal fluorescence
503 microscopy for the analyses. Because that technique does not distinguish between inside or
504 around the nucleus, the signal observed may have been perinuclear, e.g. from the
505 endoplasmic reticulum. A thorough look at phylogenetic analyses from Scutenaire *et al.* (2018)
506 reveals that *ECT1* is only present in species of the 'lineage I' of Brassicaceae such as *A.*
507 *thaliana* and *Capsella rubella* (*Cru*) (Nikolov *et al*, 2019). The closely related *Brassica oleracea*
508 ('lineage II') (Nikolov *et al.*, 2019) has a clear homolog of *Ath/Cru ECT3*, but not *ECT1*
509 (Scutenaire *et al.*, 2018), while other dicots outside *Brassicaceae* encode *ECT3/1* orthologs
510 in a separate cluster (Scutenaire *et al.*, 2018). Therefore, *ECT1* is the product of a recent
511 duplication and neofunctionalization event of the *ECT3/1* gene in a lineage of *Brassicaceae,*
512 that diverged more rapidly than any other DF-A clade member in *Arabidopsis* (Fig. 1*B*,
513 (Scutenaire *et al.*, 2018)). This agrees with our overall conclusion that most YTHDFs in early
514 angiosperms possessed *Mpo* YTHDF/*Ath* ECT2/3/4 molecular functions, and only late events
515 resulted in specialization of a few YTHDF proteins. For ECT1, this occurred late in a small
516 subgroup of dicots. We note that such rapid neofunctionalization appears to result primarily
517 from changes in the IDR. We were able to identify two biophysical properties of the IDR of
518 ECT1, a stronger predicted propensity to phase-separate and its charge distribution, that are
519 distinct from the ECT2/3/4/5/6/7/8/10 group, but note that additional changes, for example in
520 SLiMs mediating interaction with regulatory factors, may also contribute to the different
521 functionality.
522
523 *The diversity of plant YTHDF proteins and the need for many YTHDFs*
524 The observation that a few fern YTHDF proteins cluster in the angiosperm clade DF-D points
525 to an early diversification of plant YTHDFs, while the fact that some fern and gymnosperm
526 YTHDFs define an independent clade (DF-F) suggests that complex plants may need many
527 different YTHDFs, well surpassing the three paralogs found in most vertebrates (Patil *et al.*,
528 2018) or in any other types of eukaryotes (Balacco & Soller, 2019; Stoilov *et al.*, 2002). But

529 why? The need for many YTHDFs of considerable variability is all the more puzzling given our
530 demonstration here that the majority of them retains the same molecular functions.
531 Robustness is a commonly given explanation for redundancy, but the same argument could
532 apply to methyltransferase subunits, and *Arabidopsis* has maintained only one copy of *MTA*,
533 *MTB*, *FIP37*, *VIR* and *HAKAI* (Balacco & Soller, 2019). Therefore, the answer should probably
534 be sought elsewhere. It is clear now that the m^6A/YTHDF axis controls cellular proliferation
535 and organ growth in plants (Arribas-Hernández & Brodersen, 2020; Arribas-Hernández *et al.*,
536 2020), and a principal difference between animals and plants is the extreme plasticity of plant
537 growth. Because growth and stress responses are also tightly intertwined, it is possible that
538 plants use a plethora m^6A-YTHDF growth-stimulators in different organs, responsive to
539 different stresses and developmental cues, to shape plant architecture in response to stimuli.
540 The answer to the paradox may be in the details: plant YTHDFs responsive to different
541 environmental cues may fine-tune growth programs through slightly different performance and
542 target-binding capacity in partly overlapping expression domains, where they are known to
543 compete for targets (Arribas-Hernández *et al.*, 2021b).
544
545 **Materials and Methods**
546 *Plant material and growth conditions*
547 All the used lines are in the *A. thaliana* Columbia-0 (Col-0) ecotype. The T-DNA insertion lines
548 *rdr6-12* (Peragine *et al.*, 2004), *ect1-1* (SAIL_319_A08), *ect1-2* (GK-547H06), and *ect1-3*
549 (SALK_059722) were obtained from Nottingham Arabidopsis Stock Centre. The mutants *ect2-*
550 *3*, *ect3-2*, *ect2-3/ect3-2* (*Gde23*), *ect2-3/ect3-2/ect4-2* (*Gte234*) and *ect2-1/ect3-1/ect4-2*
551 (*te234*) used for genetic crosses or as background to produce transgenic lines, and the
552 primers for genotyping the corresponding alleles, have been previously described (Arribas-
553 Hernández *et al.*, 2018; Arribas-Hernández *et al.*, 2020). The standard growing conditions
554 used are detailed in Supplementary Information (SI) Materials and Methods.
555
556 *Phylogenetic analysis*
557 Amino acid sequences of selected YTH-domain proteins were downloaded from UniProt
558 (Apweiler et al., 2004), TAIR (www.arabidopsis.org), phytozome (Goodstein *et al*, 2012) or
559 GinkgoDB (Gu *et al*, 2022) and trimmed from their N-termini to discard intrinsically disordered
560 regions with poor sequence conservation, thereby retaining only the regions with conservation
561 to those structured in human YTHDF1 (Xu *et al.*, 2015) (SI Protein Sequences, Dataset S1).
562 Trimmed sequences were aligned with MUSCLE (Edgar, 2004a, b) with default parameters
563 (Dataset S2). Evolutionary analyses were conducted using IQ-Tree 2 (Minh *et al*, 2020;
564 Nguyen *et al*, 2015) from the CIPRES Science Gateway v. 3.3
565 (https://www.phylo.org/index.php/) to infer a phylogenetic tree using maximum likelihood. The

566 model based on revised JTT Matrix (Kosiol & Goldman, 2005) JTTDCMut+R5 was determined
567 as best-fit using the built-in tool ModelFinder (Kalyaanamoorthy *et al*, 2017) according to
568 Bayesian Information Criterion (BIC) scores, and used for the analysis. *Mpo* YTHDF was
569 selected as outgroup and drawn as root. Measures of branch supports by approximate
570 Likelihood Ratio Test [aLRT] (Shimodaira & Hasegawa, 1999) (SH-aLRT, %) were calculated,
571 and the resulting values were used for color-coding the nodes with the tool FigTree
572 (https://github.com/rambaut/figtree/). The precise SH-aLRT values of all nodes in newick
573 format and additional information can be found in Dataset S3.
574 Estimates of evolutionary divergence between sequences were obtained computing pairwise
575 distances among the full length sequences of the same proteins (Dataset S4), aligned in the
576 same manner (Dataset S5) using the Equal Input model (Tajima & Nei, 1984) in MEGA11
577 (Tamura *et al*, 2021). The positions containing gaps and missing data were eliminated
578 (complete deletion option), resulting a total of 180 positions in the final dataset.
579
580 *Cloning, plant transformation and line selection*
581 We employed the scar-free USER cloning method (Bitinaite & Nichols, 2009) to produce
582 *uS7Bp:cYTHDF(X)-mCherry-OCSter* and *ECT1p:gECT1-FLAG-TFP-ECT1ter* constructs by
583 gluing PCR-amplified DNA fragments into the pCAMBIA3300-U plasmid (Nour-Eldin *et al*,
584 2006) that provides resistance to glufosinate in plants. Cloning of the trial *ECT2p:gECT1-*
585 *mCherry-ECT2ter* and *ECT2p:gECT4-mCherry-ECT2ter* constructs was done by GreenGate
586 (Lampropoulos *et al*, 2013). The detailed cloning, transformation and line selection strategy
587 for each construct, as well as the specific details of T1 selections for the complementation
588 assay, are explained in SI Materials and Methods.
589
590 *IDR modeling and simulations*
591 We carried out coarse-grained simulations of protein IDRs using the implicit-solvent
592 CALVADOS 2 forcefield (Tesei & Lindorff-Larsen, 2022; Tesei *et al.*, 2021). In CALVADOS,
593 amino-acid residues are mapped to single beads corresponding to their amino-acid type.
594 Neighboring residues are linked using harmonic bonds with an equilibrium distance of 0.38
595 nm and force constant of 8033 kJ $mol^{-1}nm^{-2}$. Nonbonded interactions are modeled with a
596 hydropathy amino-acid "stickiness" model using λ-parameters from CALVADOS 2 (Tesei &
597 Lindorff-Larsen, 2022). Salt-screened electrostatic interactions are accounted for with a
598 truncated (r_c = 4 nm) and shifted Debye-Hückel potential; non-electrostatic interactions were
599 truncated at 2 nm (Tesei & Lindorff-Larsen, 2022). We used a Langevin integrator with friction
600 coefficient γ = 0.01 ps^{-1} to propagate the simulation in 0.01 ps timesteps. All simulations were
601 carried out at T = 293 K.

602 We performed slab simulations of IDRs of the following proteins: ECT1-ECT11, *Mpo*
603 YTHDF, *Hs* YTHDF2, *Dm* YTHDF1, and *Hs* FUS, using a previously described procedure
604 (Dignon *et al*, 2018; Tesei & Lindorff-Larsen, 2022). IDR sequences are detailed in SI Protein
605 Sequences. Briefly, we simulated 100 copies of each IDR (one type of IDR at a time) in a
606 simulation slab of dimensions 25 nm x 25 nm x 300 nm (ECT2, ECT4, ECT5, *Mpo* YTHDF,
607 *Hs* YTHDF2, *Dm* YTHDF), 17 nm x 17 nm x 300 nm (ECT1, ECT3, ECT6-ECT11), or 15 nm
608 x 15 nm x 150 nm (*Hs* FUS), accounting for the different IDR sequence lengths. We simulated
609 each system for 7500 ns and recorded configurations at 1 ns intervals. The first 2000 ns of
610 each simulation were considered as equilibration and not used for analysis. We centered the
611 protein condensates in the z-dimension of the simulation box during post-processing. We
612 determined concentrations of the dense phase and dilute phase by fitting the concentration
613 profiles to a hyperbolic function, as described by Tesei et al. (2021). Excess transfer free
614 energies were calculated from the dilute and dense phase equilibrium concentrations via
615 $\Delta G_{trans} = RT \ln (c_{dilute} / c_{dense})$ (Benayad *et al*, 2021).
616 Charges (q) were added along the IDR sequences to obtain cumulative charge plots.
617 Arg and Lys residues were assigned charges of q = +1; Glu and Asp residues were assigned
618 charges of q = -1; other residue types, including His, were assigned charges of q = 0. The
619 average 'stickiness' of a given IDR sequence was determined by calculating the mean
620 hydrophobicity $\bar{\lambda}$ of the IDR amino acid composition, using the CALVADOS 2 hydrophobicity
621 scale reported in (Tesei & Lindorff-Larsen, 2022).
622
623 Additional standard methods including DNA and cDNA obtention, genotyping, fluorescence
624 microscopy, qPCR, RNA and protein blotting, and the characterization of YTH domains, are
625 described in SI Materials and Methods.
626
627 **Acknowledgements and funding sources**
628 We thank Lena Bjørn Johansson, Sergio D'Anna and Tobias Lahti for technical assistance,
629 Theo Bølsterli and his team for plant care, and the Danish National Life Science
630 Supercomputing Center Computerome and the core facility for biocomputing at the
631 Department of Biology (University of Copenhagen) for the use of computational resources.
632 We acknowledge the constructive criticism of Rupert Fray as a reviewer on previous
633 publications, as his suggestion to use the *ect2/ect3/ect4* triple mutant phenotype to test ECT
634 molecular function by systematic ectopic expression in the ECT2 expression domain inspired
635 us to embark on the present project. This work was supported by the Novo Nordisk Foundation
636 through a Hallas-Møller Ascending Investigator 2019 grant NNF19OC0054973 to P.B. and an
637 NNF18OC0033950 grant to K.L.-L. via the PRISM (Protein Interactions and Stability in

638 Medicine and Genomics) center, and by the Independent Research Fund Denmark through a
639 Research Project2 grant (9040-00409B) from to P.B.
640

641 **References**
642

643 Anderson SJ, Kramer MC, Gosai SJ, Yu X, Vandivier LE, Nelson ADL, Anderson ZD, Beilstein MA,
644 Fray RG, Lyons E *et al* (2018) N(6)-Methyladenosine Inhibits Local Ribonucleolytic Cleavage to
645 Stabilize mRNAs in Arabidopsis. *Cell Rep* 25: 1146-1157

646 Arribas-Hernández L, Bressendorff S, Hansen MH, Poulsen C, Erdmann S, Brodersen P (2018) An
647 m6A-YTH Module Controls Developmental Timing and Morphogenesis in Arabidopsis. *Plant Cell* 30:
648 952-967

649 Arribas-Hernández L, Brodersen P (2020) Occurrence and functions of m6A and other covalent
650 modifications in plant mRNA. *Plant Physiol* 182: 79-96

651 Arribas-Hernández L, Rennie S, Köster T, Porcelli C, Lewinski M, Staiger D, Andersson R, Brodersen
652 P (2021a) Principles of mRNA targeting via the Arabidopsis m6A-binding protein ECT2. *eLife* 10:
653 e72375

654 Arribas-Hernández L, Rennie S, Schon M, Porcelli C, Enugutti B, Andersson R, Nodine MD, Brodersen
655 P (2021b) The YTHDF proteins ECT2 and ECT3 bind largely overlapping target sets and influence
656 target mRNA abundance, not alternative polyadenylation. *eLife* 10: e72377

657 Arribas-Hernández L, Simonini S, Hansen MH, Paredes EB, Bressendorff S, Dong Y, Østergaard L,
658 Brodersen P (2020) Recurrent requirement for the m6A-ECT2/ECT3/ECT4 axis in the control of cell
659 proliferation during plant organogenesis. *Development* 147: dev189134

660 Balacco DL, Soller M (2019) The m6A Writer: Rise of a Machine for Growing Tasks. *Biochemistry* 58:
661 363-378

662 Benayad Z, von Bülow S, Stelzl LS, Hummer G (2021) Simulation of FUS Protein Condensates with an
663 Adapted Coarse-Grained Model. *Journal of Chemical Theory and Computation* 17: 525-537

664 Bergeron-Sandoval L-P, Safaee N, Michnick Stephen W (2016) Mechanisms and Consequences of
665 Macromolecular Phase Separation. *Cell* 165: 1067-1079

666 Bianchi G, Mangiagalli M, Barbiroli A, Longhi S, Grandori R, Santambrogio C, Brocca S (2022)
667 Distribution of Charged Residues Affects the Average Size and Shape of Intrinsically Disordered
668 Proteins. *Biomolecules* doi: 10.3390/biom12040561 [PREPRINT]

669 Biasini M, Bienert S, Waterhouse A, Arnold K, Studer G, Schmidt T, Kiefer F, Cassarino TG, Bertoni M,
670 Bordoli L *et al* (2014) SWISS-MODEL: modelling protein tertiary and quaternary structure using
671 evolutionary information. *Nucleic Acids Res* 42: W252-W258

672 Bitinaite J, Nichols NM (2009) DNA cloning and engineering by uracil excision. *Curr Protoc Mol Biol*
673 Chapter 3: Unit 3 21

674 Bodi Z, Zhong S, Mehra S, Song J, Graham N, Li H, May S, Fray RG (2012) Adenosine methylation in
675 Arabidopsis mRNA is associated with the 3' end and reduced levels cause developmental defects. *Front*
676 *Plant Sci* 3: 48

677 Boo SH, Ha H, Lee Y, Shin M-K, Lee S, Kim YK (2022) UPF1 promotes rapid degradation of m6A-
678 containing RNAs. *Cell Rep* 39: 110861

679 Borcherds W, Bremer A, Borgia MB, Mittag T (2021) How do intrinsically disordered protein regions
680 encode a driving force for liquid–liquid phase separation? *Curr Opin Struct Biol* 67: 41-50

681 Bowman JL, Kohchi T, Yamato KT, Jenkins J, Shu S, Ishizaki K, Yamaoka S, Nishihama R, Nakamura
682 Y, Berger F *et al* (2017) Insights into Land Plant Evolution Garnered from the Marchantia polymorpha
683 Genome. *Cell* 171: 287-304.e215

684 Brodsky S, Jana T, Mittelman K, Chapal M, Kumar DK, Carmi M, Barkai N (2020) Intrinsically
685 Disordered Regions Direct Transcription Factor In Vivo Binding Specificity. *Mol Cell*
686 79: 459-471.e454

687 Dalmay T, Hamilton A, Rudd S, Angell S, Baulcombe DC (2000) An RNA-dependent RNA polymerase
688 gene in Arabidopsis is required for posttranscriptional gene silencing mediated by a transgene but not
689 by a virus. *Cell* 101: 543-553

690 Das RK, Huang Y, Phillips AH, Kriwacki RW, Pappu RV (2016) Cryptic sequence features within the
691 disordered protein p27Kip1 regulate cell cycle signaling. *Proc Natl Acad Sci USA* 113: 5616-5621

692 Dignon GL, Zheng W, Kim YC, Best RB, Mittal J (2018) Sequence determinants of protein phase
693 behavior from a coarse-grained model. *PLOS Computational Biology* 14: e1005941

694 Dominissini D, Moshitch-Moshkovitz S, Schwartz S, Salmon-Divon M, Ungar L, Osenberg S, Cesarkas
695 K, Jacob-Hirsch J, Amariglio N, Kupiec M *et al* (2012) Topology of the human and mouse m6A RNA
696 methylomes revealed by m6A-seq. *Nature* 485: 201-206

697 Du H, Zhao Y, He J, Zhang Y, Xi H, Liu M, Ma J, Wu L (2016) YTHDF2 destabilizes m6A-containing
698 RNA through direct recruitment of the CCR4–NOT deadenylase complex. *Nat Commun* 7: 12626

699 Edgar RC (2004a) MUSCLE: a multiple sequence alignment method with reduced time and space
700 complexity. *BMC Bioinformatics* 5: 113

701 Edgar RC (2004b) MUSCLE: multiple sequence alignment with high accuracy and high throughput.
702 *Nucleic Acids Res* 32: 1792-1797

703 Fagard M, Vaucheret H (2000) (TRANS)GENE SILENCING IN PLANTS: How Many Mechanisms?
704 *Annu Rev Plant Physiol Plant Mol Biol* 51: 167-194

705 Fray RG, Simpson GG (2015) The Arabidopsis epitranscriptome. *Curr Opin Plant Biol* 27: 17-21

706 Fu Y, Zhuang X (2020) m6A-binding YTHDF proteins promote stress granule formation. *Nat Chem Biol*
707 16: 955-963

708 Gan S (2003) Mitotic and Postmitotic Senescence in Plants. *Science of Aging Knowledge Environment*
709 2003: re7-re7

710 Gao Y, Pei G, Li D, Li R, Shao Y, Zhang QC, Li P (2019) Multivalent m6A motifs promote phase
711 separation of YTHDF proteins. *Cell Res* 29: 767-769

712 Geula S, Moshitch-Moshkovitz S, Dominissini D, Mansour AA, Kol N, Salmon-Divon M, Hershkovitz V,
713 Peer E, Mor N, Manor YS *et al* (2015) m6A mRNA methylation facilitates resolution of naïve pluripotency
714 toward differentiation. *Science* 347: 1002-1006

715 Goodstein DM, Shu S, Howson R, Neupane R, Hayes RD, Fazo J, Mitros T, Dirks W, Hellsten U,
716 Putnam N *et al* (2012) Phytozome: a comparative platform for green plant genomics. *Nucleic Acids Res*
717 40: D1178-D1186

718 Gu K-J, Lin C-F, Wu J-J, Zhao Y-P (2022) GinkgoDB: an ecological genome database for the living
719 fossil, Ginkgo biloba. *Database* 2022: baac046

720 Harris BJ, Harrison CJ, Hetherington AM, Williams TA (2020) Phylogenomic Evidence for the
721 Monophyly of Bryophytes and the Reductive Evolution of Stomata. *Current Biology* 30: 2001-
722 2012.e2002

723 Haussmann IU, Bodi Z, Sanchez-Moran E, Mongan NP, Archer N, Fray RG, Soller M (2016) m6A
724 potentiates Sxl alternative pre-mRNA splicing for robust Drosophila sex determination. *Nature* 540: 301

725 Herzog VA, Reichholf B, Neumann T, Rescheneder P, Bhat P, Burkard TR, Wlotzka W, von Haeseler
726 A, Zuber J, Ameres SL (2017) Thiol-linked alkylation of RNA to assess expression dynamics. *Nat Meth*
727 14: 1198

728 Ivanova I, Much C, Di Giacomo M, Azzi C, Morgan M, Moreira PN, Monahan J, Carrieri C, Enright AJ,
729 O'Carroll D (2017) The RNA m6A reader YTHDF2 is essential for the post-transcriptional regulation of
730 the maternal transcriptome and oocyte competence. *Mol Cell* 67: 1059-1067

731 Jumper J, Evans R, Pritzel A, Green T, Figurnov M, Ronneberger O, Tunyasuvunakool K, Bates R,
732 Žídek A, Potapenko A *et al* (2021) Highly accurate protein structure prediction with AlphaFold. *Nature*
733 596: 583-589

734 Kalyaanamoorthy S, Minh BQ, Wong TKF, von Haeseler A, Jermiin LS (2017) ModelFinder: fast model
735 selection for accurate phylogenetic estimates. *Nat Meth* 14: 587-589

736 Kato M, Han TW, Xie S, Shi K, Du X, Wu LC, Mirzaei H, Goldsmith EJ, Longgood J, Pei J *et al* (2012)
737 Cell-free formation of RNA granules: low complexity sequence domains form dynamic fibers within
738 hydrogels. *Cell* 149: 753-767

739 Kato M, McKnight SL (2021) The low-complexity domain of the FUS RNA binding protein self-
740 assembles via the mutually exclusive use of two distinct cross-β cores. *Proc Natl Acad Sci USA* 118:
741 e2114412118

742 Ke S, Pandya-Jones A, Saito Y, Fak JJ, Vågbø CB, Geula S, Hanna JH, Black DL, Darnell JE, Darnell
743 RB (2017) m6A mRNA modifications are deposited in nascent pre-mRNA and are not required for
744 splicing but do specify cytoplasmic turnover. *Genes Dev* 31: 990-1006

745 Kontur C, Jeong M, Cifuentes D, Giraldez AJ (2020) Ythdf m6A Readers Function Redundantly during
746 Zebrafish Development. *Cell Rep* 33: 108598

747 Kosiol C, Goldman N (2005) Different Versions of the Dayhoff Rate Matrix. *Mol Biol Evol* 22: 193-199

748 Lampropoulos A, Sutikovic Z, Wenzl C, Maegele I, Lohmann JU, Forner J (2013) GreenGate - A Novel,
749 Versatile, and Efficient Cloning System for Plant Transgenesis. *PLOS ONE* 8: e83043

750 Lan T, Xiong W, Chen X, Mo B, Tang G (2022) Plant cytoplasmic ribosomal proteins: an update on
751 classification, nomenclature, evolution and resources. *Plant J* 110: 292-318

752 Lasman L, Krupalnik V, Viukov S, Mor N, Aguilera-Castrejon A, Schneir D, Bayerl J, Mizrahi O, Peles
753 S, Tawil S *et al* (2020) Context-dependent functional compensation between Ythdf m6A reader proteins.
754 *Genes Dev* 34: 1373-1391

755 Lence T, Akhtar J, Bayer M, Schmid K, Spindler L, Ho CH, Kreim N, Andrade-Navarro MA, Poeck B,
756 Helm M *et al* (2016) m6A modulates neuronal functions and sex determination in Drosophila. *Nature*
757 540: 242

758 Li A, Chen Y-S, Ping X-L, Yang X, Xiao W, Yang Y, Sun H-Y, Zhu Q, Baidya P, Wang X *et al* (2017)
759 Cytoplasmic m6A reader YTHDF3 promotes mRNA translation. *Cell Res* 27: 444

760 Li D, Zhang H, Hong Y, Huang L, Li X, Zhang Y, Ouyang Z, Song F (2014a) Genome-wide identification,
761 biochemical characterization, and expression analyses of the YTH domain-containing RNA-binding
762 protein family in Arabidopsis and rice. *Plant Mol Biol Report* 32: 1169-1186

763 Li F, Zhao D, Wu J, Shi Y (2014b) Structure of the YTH domain of human YTHDF2 in complex with an
764 m6A mononucleotide reveals an aromatic cage for m6A recognition. *Cell Res* 24: 1490-1492

765 Li F-W, Nishiyama T, Waller M, Frangedakis E, Keller J, Li Z, Fernandez-Pozo N, Barker MS, Bennett
766 T, Blázquez MA *et al* (2020) Anthoceros genomes illuminate the origin of land plants and the unique
767 biology of hornworts. *Nature plants* 6: 259-272

768 Li M, Zhao X, Wang W, Shi H, Pan Q, Lu Z, Perez SP, Suganthan R, He C, Bjørås M *et al* (2018)
769 Ythdf2-mediated m6A mRNA clearance modulates neural development in mice. *Genome biology* 19:
770 69

771 Liu N, Dai Q, Zheng G, He C, Parisien M, Pan T (2015) N6-methyladenosine-dependent RNA structural
772 switches regulate RNA-protein interactions. *Nature* 518: 560-564

773 Luo S, Tong L (2014) Molecular basis for the recognition of methylated adenines in RNA by the
774 eukaryotic YTH domain. *Proc Natl Acad Sci USA* 111: 13834-13839

775 Magallón S, Hilu KW, Quandt D (2013) Land plant evolutionary timeline: Gene effects are secondary to
776 fossil constraints in relaxed clock estimation of age and substitution rates. *Am J Bot* 100: 556-573

777 Minh BQ, Schmidt HA, Chernomor O, Schrempf D, Woodhams MD, von Haeseler A, Lanfear R (2020)
778 IQ-TREE 2: New Models and Efficient Methods for Phylogenetic Inference in the Genomic Era. *Mol Biol*
779 *Evol* 37: 1530-1534

780 Mourrain P, Beclin C, Elmayan T, Feuerbach F, Godon C, Morel J-B, Jouette D, Lacombe A-M, Nikic
781 S, Picault N *et al* (2000) *Arabidopsis SGS2* and *SGS3* genes are required for posttranscriptional gene
782 silencing and natural virus resistance. *Cell* 101: 533-542

783 Nguyen L-T, Schmidt HA, von Haeseler A, Minh BQ (2015) IQ-TREE: A Fast and Effective Stochastic
784 Algorithm for Estimating Maximum-Likelihood Phylogenies. *Mol Biol Evol* 32: 268-274

785 Nikolov LA, Shushkov P, Nevado B, Gan X, Al-Shehbaz IA, Filatov D, Bailey CD, Tsiantis M (2019)
786 Resolving the backbone of the Brassicaceae phylogeny for investigating trait diversity. *New Phytol* 222:
787 1638-1651

788 Nour-Eldin HH, Hansen BG, Norholm MH, Jensen JK, Halkier BA (2006) Advancing uracil-excision
789 based cloning towards an ideal technique for cloning PCR fragments. *Nucleic Acids Res* 34: e122

790 Ok SH, Jeong HJ, Bae JM, Shin JS, Luan S, Kim KN (2005) Novel CIPK1-associated proteins in
791 Arabidopsis contain an evolutionarily conserved C-terminal region that mediates nuclear localization.
792 *Plant Physiol* 139: 138-150

793 One Thousand Plant Transcriptomes I (2019) One thousand plant transcriptomes and
794 the phylogenomics of green plants. *Nature* 574: 679-685

795 Park OH, Ha H, Lee Y, Boo SH, Kwon DH, Song HK, Kim YK (2019) Endoribonucleolytic Cleavage of
796 m6A-Containing RNAs by RNase P/MRP Complex. *Mol Cell* 74: 494-507.e498

797 Parker MT, Knop K, Sherwood AV, Schurch NJ, Mackinnon K, Gould PD, Hall AJW, Barton GJ,
798 Simpson GG (2020) Nanopore direct RNA sequencing maps the complexity of Arabidopsis mRNA
799 processing and m6A modification. *eLife* 9: e49658

800 Patel A, Lee Hyun O, Jawerth L, Maharana S, Jahnel M, Hein Marco Y, Stoynov S, Mahamid J, Saha
801 S, Franzmann Titus M *et al* (2015) A Liquid-to-Solid Phase Transition of the ALS Protein FUS
802 Accelerated by Disease Mutation. *Cell* 162: 1066-1077

803 Patil DP, Pickering BF, Jaffrey SR (2018) Reading m6A in the Transcriptome: m6A-Binding Proteins.
804 *Trends Cell Biol* 28: 113-127

Peragine A, Yoshikawa M, Wu G, Albrecht HL, Poethig RS (2004) SGS3 and SGS2/SDE1/RDR6 are required for juvenile development and the production of trans-acting siRNAs in Arabidopsis. *Genes Dev* 18: 2368-2379

Piovesan D, Del Conte A, Clementel D, Monzon Alexander M, Bevilacqua M, Aspromonte Maria C, Iserte Javier A, Orti FE, Marino-Buslje C, Tosatto Silvio CE (2023) MobiDB: 10 years of intrinsically disordered proteins. *Nucleic Acids Res* 51: D438-D444

Pires ND, Dolan L (2012) Morphological evolution in land plants: new designs with old genes. *Philosophical Transactions of the Royal Society B: Biological Sciences* 367: 508-518

Puttick MN, Morris JL, Williams TA, Cox CJ, Edwards D, Kenrick P, Pressel S, Wellman CH, Schneider H, Pisani D *et al* (2018) The Interrelationships of Land Plants and the Nature of the Ancestral Embryophyte. *Current Biology* 28: 733-745.e732

Ries RJ, Zaccara S, Klein P, Olarerin-George A, Namkoong S, Pickering BF, Patil DP, Kwak H, Lee JH, Jaffrey SR (2019) m6A enhances the phase separation potential of mRNA. *Nature* 571: 424-428

Roost C, Lynch SR, Batista PJ, Qu K, Chang HY, Kool ET (2015) Structure and Thermodynamics of N6-Methyladenosine in RNA: A Spring-Loaded Base Modification. *J Am Chem Soc* 137: 2107-2115

Růžička K, Zhang M, Campilho A, Bodi Z, Kashif M, Saleh M, Eeckhout D, El-Showk S, Li H, Zhong S *et al* (2017) Identification of factors required for m6A mRNA methylation in Arabidopsis reveals a role for the conserved E3 ubiquitin ligase HAKAI. *New Phytol* 215: 157-172

Schwartz Jacob C, Wang X, Podell Elaine R, Cech Thomas R (2013) RNA Seeds Higher-Order Assembly of FUS Protein. *Cell Rep* 5: 918-925

Scutenaire J, Deragon J-M, Jean V, Benhamed M, Raynaud C, Favory J-J, Merret R, Bousquet-Antonelli C (2018) The YTH Domain Protein ECT2 Is an m6A Reader Required for Normal Trichome Branching in Arabidopsis. *Plant Cell* 30: 986-1005

Scutenaire J, Plassard D, Matelot M, Villa T, Zumsteg J, Libri D, Séraphin B (2022) The S. cerevisiae m6A-reader Pho92 promotes timely meiotic recombination by controlling key methylated transcripts. *Nucleic Acids Res*: gkac640

Shen L, Liang Z, Gu X, Chen Y, Teo Zhi Wei N, Hou X, Cai Weiling M, Dedon Peter C, Liu L, Yu H (2016) N6-methyladenosine RNA modification regulates shoot stem cell fate in Arabidopsis. *Dev Cell* 38: 186-200

Shi H, Wang X, Lu Z, Zhao BS, Ma H, Hsu PJ, Liu C, He C (2017) YTHDF3 facilitates translation and decay of N6-methyladenosine-modified RNA. *Cell Res* 27: 315-328

Shi H, Zhang X, Weng Y-L, Lu Z, Liu Y, Lu Z, Li J, Hao P, Zhang Y, Zhang F *et al* (2018) m6A facilitates hippocampus-dependent learning and memory through YTHDF1. *Nature* 563: 249-253

Shimodaira H, Hasegawa M (1999) Multiple Comparisons of Log-Likelihoods with Applications to Phylogenetic Inference. *Mol Biol Evol* 16: 1114-1114

Sommer S, Lavi U, Darnell JE (1978) The absolute frequency of labeled N-6-methyladenosine in HeLa cell messenger RNA decreases with label time. *Journal of Molecular Biology* 124: 487-499

Spitale RC, Flynn RA, Zhang QC, Crisalli P, Lee B, Jung J-W, Kuchelmeister HY, Batista PJ, Torre EA, Kool ET *et al* (2015) Structural imprints in vivo decode RNA regulatory mechanisms. *Nature* 519: 486-490

Stoilov P, Rafalska I, Stamm S (2002) YTH: a new domain in nuclear proteins. *Trends Biochem Sci* 27: 495-497

847 Su D, Yang L, Shi X, Ma X, Zhou X, Hedges SB, Zhong B (2021) Large-Scale Phylogenomic Analyses
848 Reveal the Monophyly of Bryophytes and Neoproterozoic Origin of Land Plants. *Mol Biol Evol* 38: 3332-
849 3344

850 Tajima F, Nei M (1984) Estimation of evolutionary distance between nucleotide sequences. *Mol Biol*
851 *Evol* 1: 269-285

852 Tamura K, Stecher G, Kumar S (2021) MEGA11: Molecular Evolutionary Genetics Analysis Version 11.
853 *Mol Biol Evol* 38: 3022-3027

854 Tesei G, Lindorff-Larsen K, 2022. Improved Predictions of Phase Behaviour of Intrinsically Disordered
855 Proteins by Tuning the Interaction Range. bioRxiv.

856 Tesei G, Schulze TK, Crehuet R, Lindorff-Larsen K (2021) Accurate model of liquid-liquid phase
857 behavior of intrinsically disordered proteins from optimization of single-chain properties. *Proc Natl Acad*
858 *Sci USA* 118: e2111696118

859 Theler D, Dominguez C, Blatter M, Boudet J, Allain FH (2014) Solution structure of the YTH domain in
860 complex with N6-methyladenosine RNA: a reader of methylated RNA. *Nucleic Acids Res* 42: 13911-
861 13919

862 Varadi M, Anyango S, Deshpande M, Nair S, Natassia C, Yordanova G, Yuan D, Stroe O, Wood G,
863 Laydon A *et al* (2022) AlphaFold Protein Structure Database: massively expanding the structural
864 coverage of protein-sequence space with high-accuracy models. *Nucleic Acids Res* 50: D439-D444

865 Varier RA, Sideri T, Capitanchik C, Manova Z, Calvani E, Rossi A, Edupuganti RR, Ensinck I, Chan
866 VWC, Patel H *et al* (2022) N6-methyladenosine (m6A) reader Pho92 is recruited co-transcriptionally
867 and couples translation to mRNA decay to promote meiotic fitness in yeast. *eLife* 11: e84034

868 Wang C, Zhu Y, Bao H, Jiang Y, Xu C, Wu J, Shi Y (2016) A novel RNA-binding mode of the YTH
869 domain reveals the mechanism for recognition of determinant of selective removal by Mmi1. *Nucleic*
870 *Acids Res* 44: 969-982

871 Wang J, Wang L, Diao J, Shi YG, Shi Y, Ma H, Shen H (2020) Binding to m6A RNA promotes YTHDF2-
872 mediated phase separation. *Protein & Cell* 11: 304-307

873 Wang L, Roossinck MJ (2006) Comparative analysis of expressed sequences reveals a conserved
874 pattern of optimal codon usage in plants. *Plant Mol Biol* 61: 699-710

875 Wang X, Lu Z, Gomez A, Hon GC, Yue Y, Han D, Fu Y, Parisien M, Dai Q, Jia G *et al* (2014a) N6-
876 methyladenosine-dependent regulation of messenger RNA stability. *Nature* 505: 117-120

877 Wang X, Zhao Boxuan S, Roundtree Ian A, Lu Z, Han D, Ma H, Weng X, Chen K, Shi H, He C (2015)
878 N6-methyladenosine modulates messenger RNA translation efficiency. *Cell* 161: 1388-1399

879 Wang Y, Li Y, Toth JI, Petroski MD, Zhang Z, Zhao JC (2014b) N6-methyladenosine modification
880 destabilizes developmental regulators in embryonic stem cells. *Nature cell biology* 16: 191-198

881 Wei L-H, Song P, Wang Y, Lu Z, Tang Q, Yu Q, Xiao Y, Zhang X, Duan H-C, Jia G (2018) The m6A
882 Reader ECT2 Controls Trichome Morphology by Affecting mRNA Stability in Arabidopsis. *Plant Cell* 30:
883 968-985

884 Weijers D, Franke-van Dijk M, Vencken R-J, Quint A, Hooykaas P, Offringa R (2001) An Arabidopsis
885 Minute-like phenotype caused by a semi-dominant mutation in a RIBOSOMAL PROTEIN S5 gene.
886 *Development* 128: 4289-4299

887 Wuest SE, Philipp MA, Guthörl D, Schmid B, Grossniklaus U (2016) Seed Production Affects Maternal
888 Growth and Senescence in Arabidopsis *Plant Physiol* 171: 392-404

889 Xu C, Liu K, Ahmed H, Loppnau P, Schapira M, Min J (2015) Structural Basis for the Discriminative
890 Recognition of N6-Methyladenosine RNA by the Human YT521-B Homology Domain Family of
891 Proteins. *Journal of Biological Chemistry* 290: 24902-24913

892 Xu C, Wang X, Liu K, Roundtree IA, Tempel W, Li Y, Lu Z, He C, Min J (2014) Structural basis for
893 selective binding of m6A RNA by the YTHDC1 YTH domain. *Nat Chem Biol* 10: 927-929

894 Zaccara S, Jaffrey SR (2020) A Unified Model for the Function of YTHDF Proteins in Regulating m(6)A-
895 Modified mRNA. *Cell* 181: 1582-1595.e1518

896 Zhang H, Zhang F, Yu Y, Feng L, Jia J, Liu B, Li B, Guo H, Zhai J (2020a) A Comprehensive Online
897 Database for Exploring ~20,000 Public Arabidopsis RNA-Seq Libraries. *Molecular Plant* 13: 1231-1233

898 Zhang J, Fu X-X, Li R-Q, Zhao X, Liu Y, Li M-H, Zwaenepoel A, Ma H, Goffinet B, Guan Y-L *et al*
899 (2020b) The hornwort genome and early land plant evolution. *Nature plants* 6: 107-118

900 Zhang Z, Theler D, Kaminska KH, Hiller M, de la Grange P, Pudimat R, Rafalska I, Heinrich B, Bujnicki
901 JM, Allain FHT *et al* (2010) The YTH domain is a novel RNA binding domain. *The Journal of biological*
902 *chemistry* 285: 14701-14710

903 Zhong S, Li H, Bodi Z, Button J, Vespa L, Herzog M, Fray RG (2008) MTA is an Arabidopsis messenger
904 RNA adenosine methylase and interacts with a homolog of a sex-specific splicing factor. *Plant Cell* 20:
905 1278-1288

906 Zhu T, Roundtree IA, Wang P, Wang X, Wang L, Sun C, Tian Y, Li J, He C, Xu Y (2014) Crystal structure
907 of the YTH domain of YTHDF2 reveals mechanism for recognition of N6-methyladenosine. *Cell Res*
908 24: 1493-1496
909

910

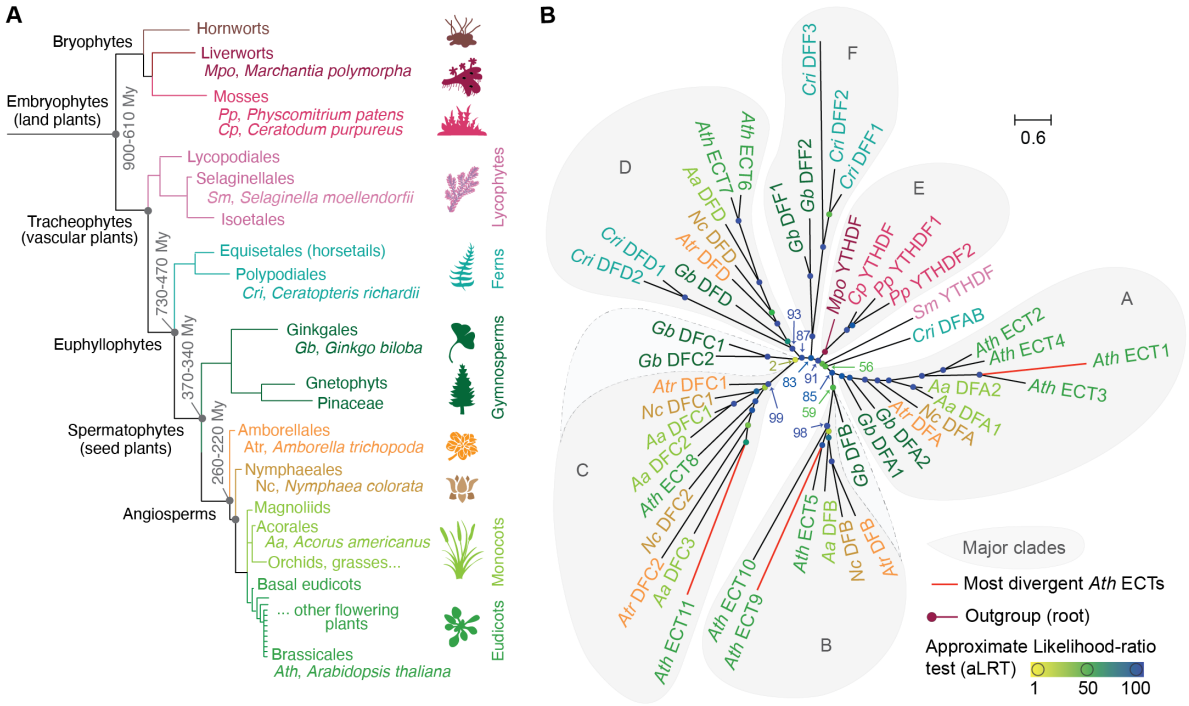

Fig. 1. Phylogenetic analysis of YTHDF proteins in land plants. (*A*) Schematic representation of land plant evolution and relative position of the species used in this study. The architecture of the diagram and the age (million years, My) indicated on some nodes are a simplified version of the tree from Su et al. (Su *et al.*, 2021). The length of the branches has been adjusted for illustrative purposes. (*B*) Phylogenetic tree of YTHDF proteins in land plants based on the sequence alignment of regions with homology to the structured regions of the metazoan orthologs (Xu *et al.*, 2015) (Datasets S1, S2). *Marchantia polymorpha* (Mpo) YTHDF is chosen as outgroup. *Arabidopsis thaliana* (*Ath*) YTHDF proteins are named after the original nomenclature for proteins containing an Evolutionarily Conserved C-Terminal Region (ECT) established by Ok et al. (Ok *et al.*, 2005). Proteins from other plant species adhere to the nomenclature established by Scutenaire et al. (Scutenaire *et al.*, 2018), with small variations reflecting additional clades (DF-E, -F) and the split of the original DF-C clade into -C and -D. Statistical support is calculated as approximate likelihood-ratio test (aLRT) and indicated by colour-coded spheres on all nodes, but the most relevant values are specified. The length of the branches represents the evolutionary distance in number of amino acid substitutions per site relative to the scale bar. Color-coding and abbreviations of species as in *A*. Dotted lines highlight weakly supported affiliations to clades.

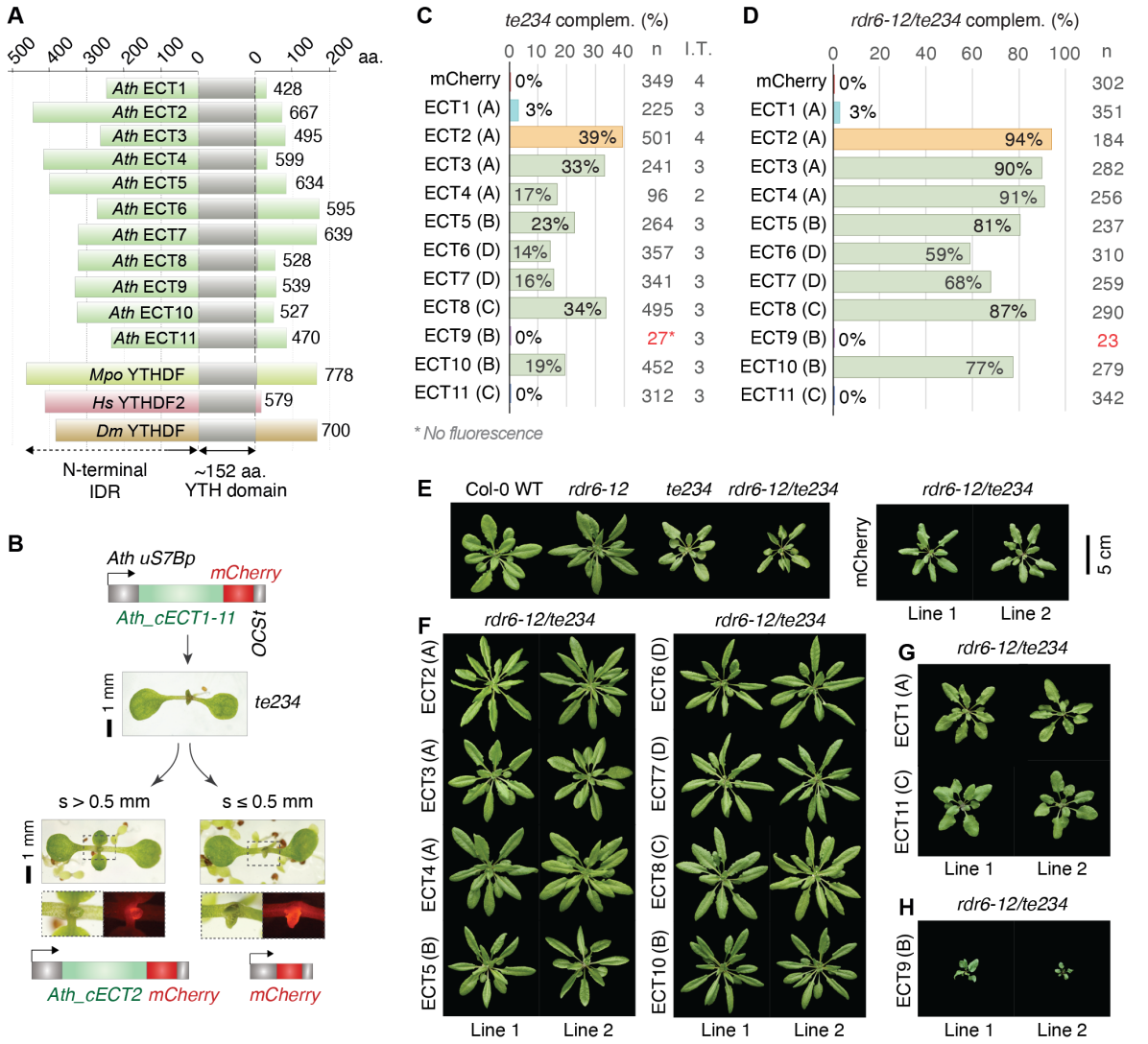

Fig. 2. Most but not all arabidopsis YTHDF proteins can replace ECT2/3/4-function. (*A*) Diagram showing the relative length of the N-terminal IDRs of *Arabidopsis thaliana* (*Ath*) YTHDF proteins (ECT1-ECT11) together with *Marchantia polymorpha* (*Mpo*) YTHDF, *Homo sapiens* (*Hs*) YTHDF2, and *Drosphila melanogaster* (*Dm*) YTHDF. Numbers indicate the length of the proteins in amino acids (aa). (*B*) Strategy followed for the functional assay. *uS7Bp:cECT(X)-mCherry* constructs are introduced in *ect2-1/ect3-1/ect4-2* (*te234*) plants, and complementation rates are estimated by the percentage of primary transformants (T1) whose first true leaves have a size (s) exceeding 0.5 mm after 10 days of growth. The *construct uS7Bp:mCherry* is used as negative control. Examples of T1 seedlings expressing control and ECT2 constructs are shown. Dashed outlines are magnified below to show mCherry fluorescence in emerging leaves. (*C*) Weighed averages of the complementation percentages observed for each *uS7Bp:cECT(X)-mCherry* construct in 2-5 independent transformations (I.T.). Letters between parenthesis indicate the DF- clade assigned to each protein. Coloring highlights ECT2 (reference) and proteins with low or negligible complementation capacity (ECT1/9/11) for fast identification along the manuscript. Low transformation efficiency (T.E.) for ECT9 can be infered by the low number of transformants (n) highlighted in red, but detailed T.E. and raw complementation rates in each transformation can be found in Figs. S5 and S3A respectively. Additional data regarding this assay is shown in Fig. S4. (*D*) Same as C on a single transformation using the *rdr6-12/te234* background. (*E-H*) Rosette phenotype of 32-day old T1s bearing *uS7Bp:cECT(X)-mCherry* constructs in the *rdr6-12/te234* background, sorted according to their degree of complementation in three panels: *F* (high), *G* (residual) and *H* (non-complementation and enhancement). Different genetic backgrounds and control transformants (mCherry) are shown in *E* as a reference. The scalebar (5 cm) applies to all plants in the four panels.

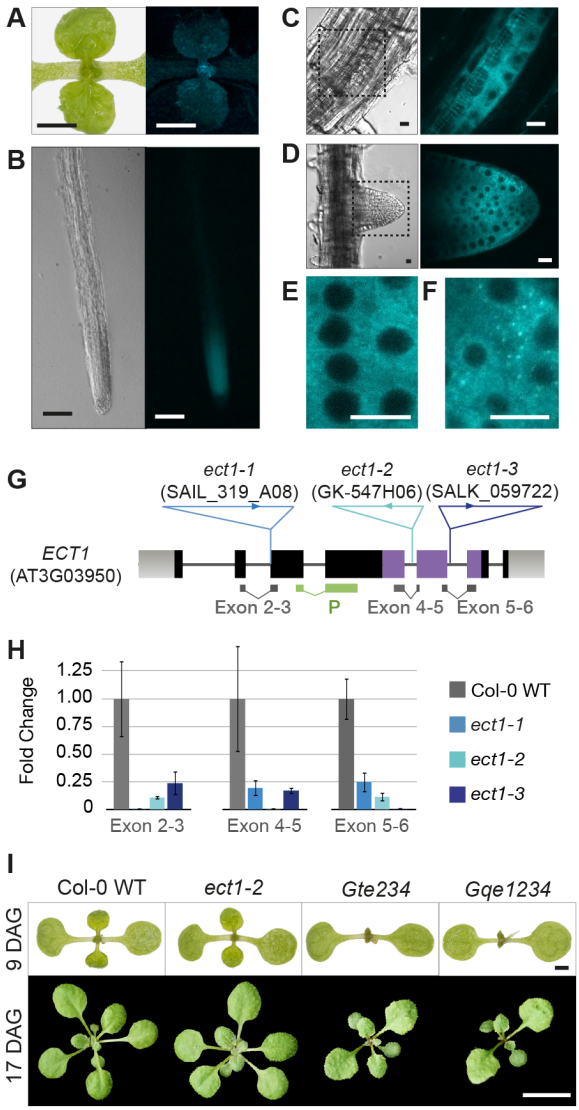

Fig. 3. Endogenous ECT1 has negligible ECT2/3/4-like function, despite similar expression pattern and subcellular localization. (*A-D*) Expression pattern of *ECT1p:gECT1-TFP* (gDNA) in aerial organs (*A*), main root (*B*), lateral root primordia (*C*) and emerging lateral roots (*D*) of 10-day-old seedlings. The expression mimics the pattern observed for ECT2/3/4 (Arribas-Hernández et al., 2020). (*E-F*) Intracellular localization of ECT1-TFP in meristematic cells of root tips in unchallegended conditions. Although the cytoplasmic signal is largely homogenous (*E*), sporadic foci (*F*) are frequently observed. Fig. S10A shows the integrity of the fluorescently tagged protein in independent transgenic lines assessed by protein blot. (*G*) Schematic representation of the *ECT1* locus. Exons are represented as boxes and introns as lines. The positions and identifiers of the T-DNA insertions assigned to the *ect1-1*, *ect1-2* and *ect1-3* alleles are marked, and the location of qPCR amplicons and hybridization probes (P) for analyses is indicated below. (*H*) Expression analysis of *ECT1* mRNA in wild type and T-DNA insertion lines by qPCR. Northern blot using the probe (P) marked in G detects *ECT1-TFP* mRNA, but not the endogenous *ECT1* transcript (Fig. S10B). (*I*) Morphological appearance of seedlings with or without *ECT1* in the different backgrounds indicated. Alternative allele combinations are shown in Fig. S10D. DAG, days after germination. Scale bars are: 1 cm in A, 1 mm in B, 100 µm in C, 10 µm in D-F, 1 mm in upper panels of I, and 1 cm in the lower panels.

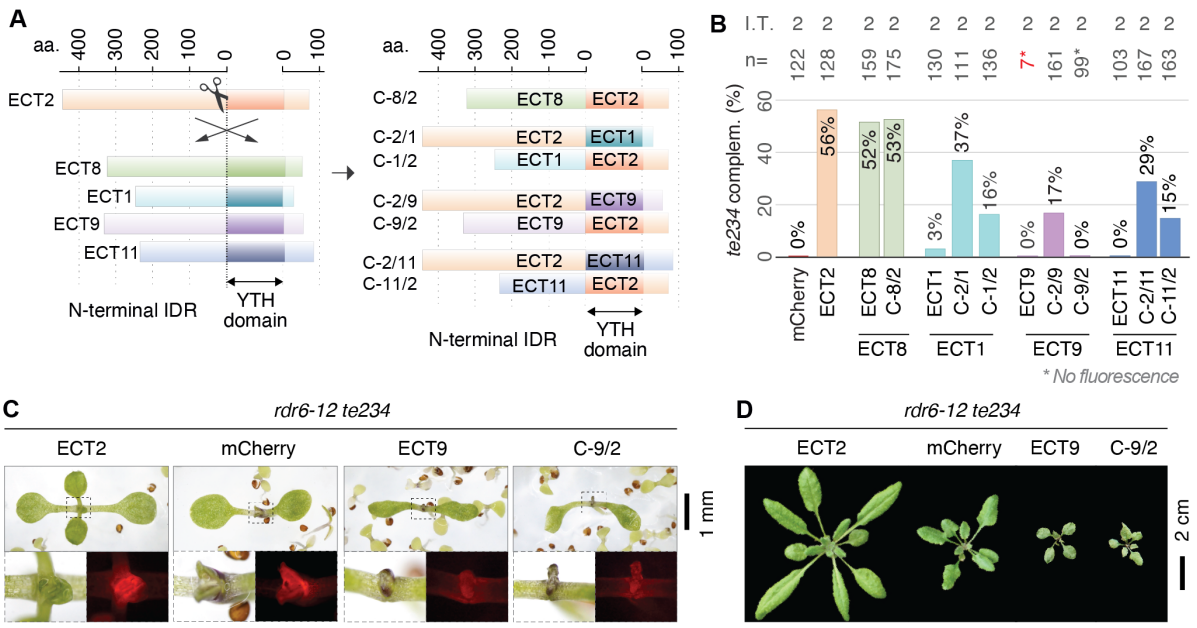

Fig. 4. Dissection of ECT1/9/11 functional regions. (*A*) Schematic representation of the strategy followed to express chimeras with N-terminal IDR and YTH domains of different ECT proteins. (*B*) Weighed averages of the complementation rates observed for each chimeric construct measured as in Fig. 2B,C. The raw complementation rates and transformation efficiencies of each independent transformation (I.T.) can be found in Figs. S3B and S5 respectively, and photographs of the scored 10-day-old T1 seedlings with mCherry fluorescence are shown in Fig. S8. (*C*) 10-day-old primary transformants of *rdr6-12/te234* with the indicated transgenes. Dashed outlines are magnified below to show mCherry fluorescencece. (*D*) Same genotypes as in C at 26 days after germination. Additional independent transgenic lines, developmental stages and controls for *C* and *D* can be found in Fig. S6. All transgenes are expressed from the *uS7B* promoter and contain mCherry fused to the C-terminus.

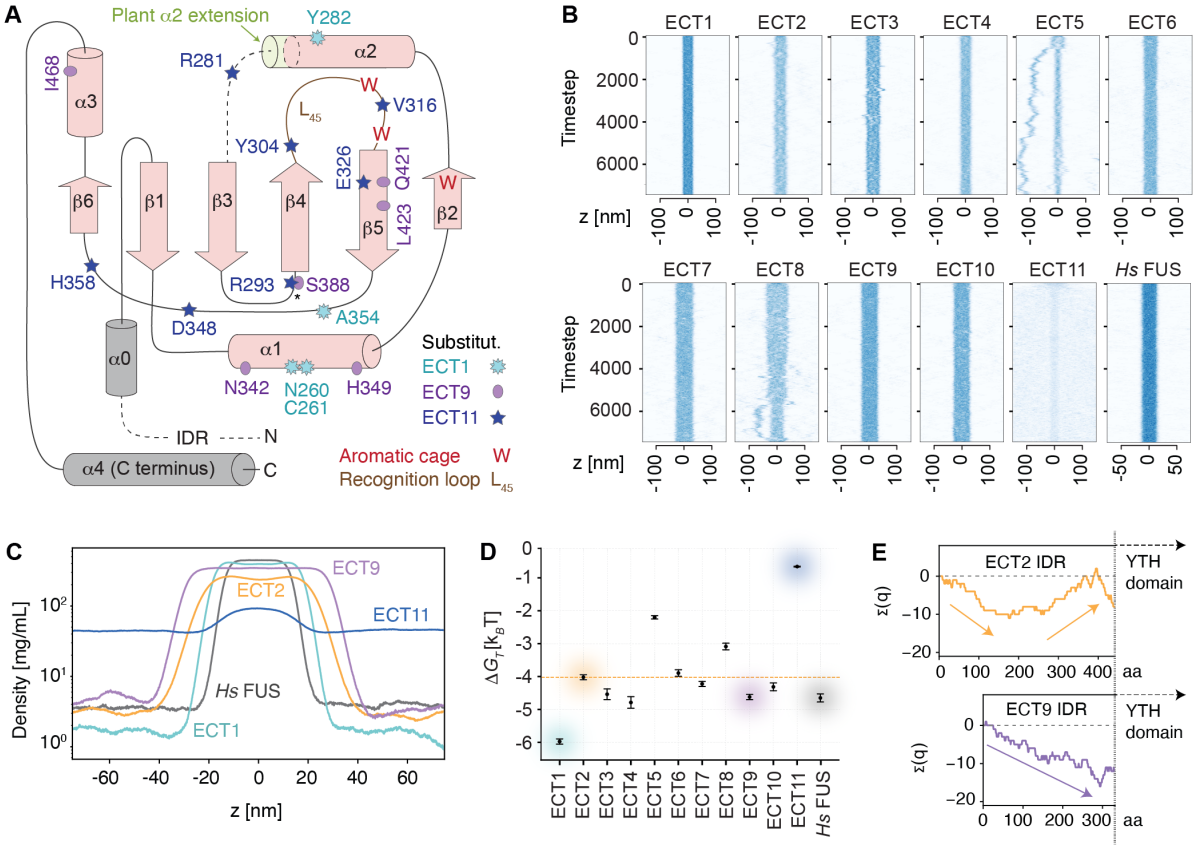

Fig. 5. Analysis of ECT1/9/11 functional regions. (*A*) Topology of the YTH domain of *Homo sapiens* (*Hs*) YTHDF1 with secondary structure elements drawn in pink (Xu *et al.*, 2015). The two grey helices represent the only structural elements outside the YTH domain (as defined by Stoilov et al. (Stoilov *et al.*, 2002)): α0 immediately upstream, and α4 at the C-terminus of the protein. Superimposed on the diagrams are the amino acids in ECT1, ECT9 and ECT11 that constitute non-conservative substitutions compared to the majority of ECTs (see alignment in Fig. S11). The localization of these amino acids in the predicted 3D structures, predominantly on the surface, and the spatial integrity of the aromatic cage in the homology models of ECT1/9/11 can be found in Fig. S12. (*B*) Slab simulations of the IDRs of the indicated proteins showing their tendency to remain in condensed phase or disperse in solution. (*C*) Time-averaged density profiles for a selected group of the slab simulations shown in B. The remaining proteins are shown in Fig. S14A. (*D*) Calculated free energy change for the transition between aqueous solution and condensed phase ($\Delta G_{trans} = RT \ln (c_{dilute} / c_{dense})$) for the IDRs of the indicated proteins. (*E*) Cumulative charge distribution of the IDRs of the indicated proteins. The length in amino acids (aa) is at scale. The same analysis for all ECTs can be found in Fig. S14D.

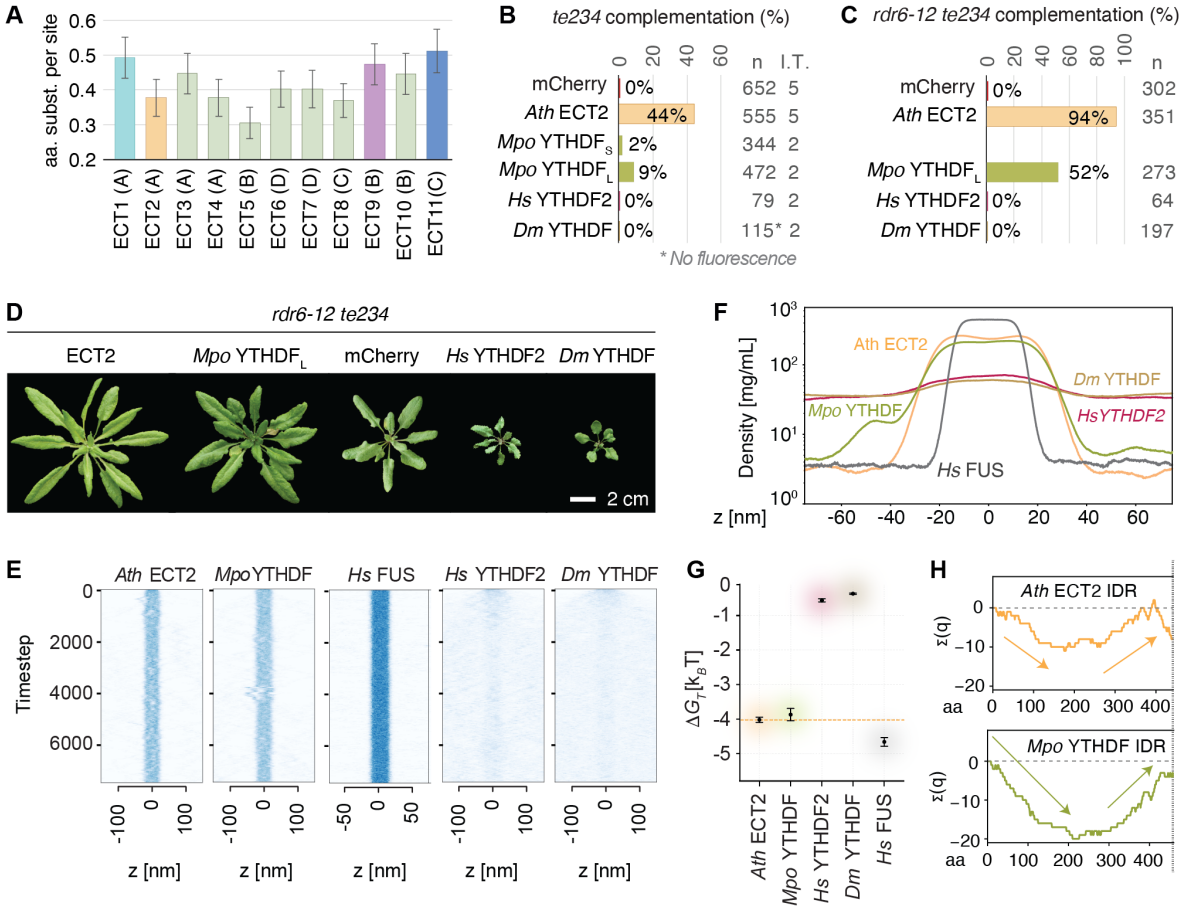

Fig. 6. Heterologous expression of *Marchantia polymorpha* (*Mpo*) YTHDF in arabidopsis rescues loss of ECT2/3/4 function, while *Homo sapiens* (*Hs*) or *Drosophila melanogaster* (*Dm*) YTHDF proteins aggravates it. (*A*) Evolutionary divergence among ECT proteins estimated by pairwise comparison of the proteins analyzed in Fig. 1B. (*B*) Weighed averages of the complementation rates observed for each of the indicated constructs (cDNA fused to mCherry under the control of the *uS7B* promoter) as in Fig. 2C in the te234 background. S (short) and L (long) refer to the two different YTHDF spliceforms found among *M. polymorpha* cDNAs. Transformation efficiencies and raw complementation rates in each transformation can be found in Figs. S5 and S3 respectively. (*C*) Same as in B but from one transformation in the *rdr6-12/te234* background. (*D*) 32-day-old primary transformants of *rdr6-12/te234* expressing the heterologous transgenes. Additional controls and developmental stages are shown in Fig. S6. (*E*) Slab simulations of the IDRs of the indicated proteins as in Fig. 5B. (*F*) Time-averaged density profiles for the slab simulations in *E*. (*G*) Calculated free energy change for the IDRs of the indicated proteins as in Fig. 5D. (*H*) Cumulative charge distribution of the IDRs of the indicated proteins as in Fig. 5E. The same analysis for all arabidopsis ECTs and animal YTHDFs can be found in Fig. S14D.